September 4, 2007

Self-assembly of nanoparticles at interfaces

Alexander Böker
Jinbo He
Thomas P. Russell
Todd S. Emrick, *University of Massachusetts - Amherst*

Soft Matter

www.softmatter.org

Volume 3 | Number 10 | 7 October 2007 | Pages 1205–1320

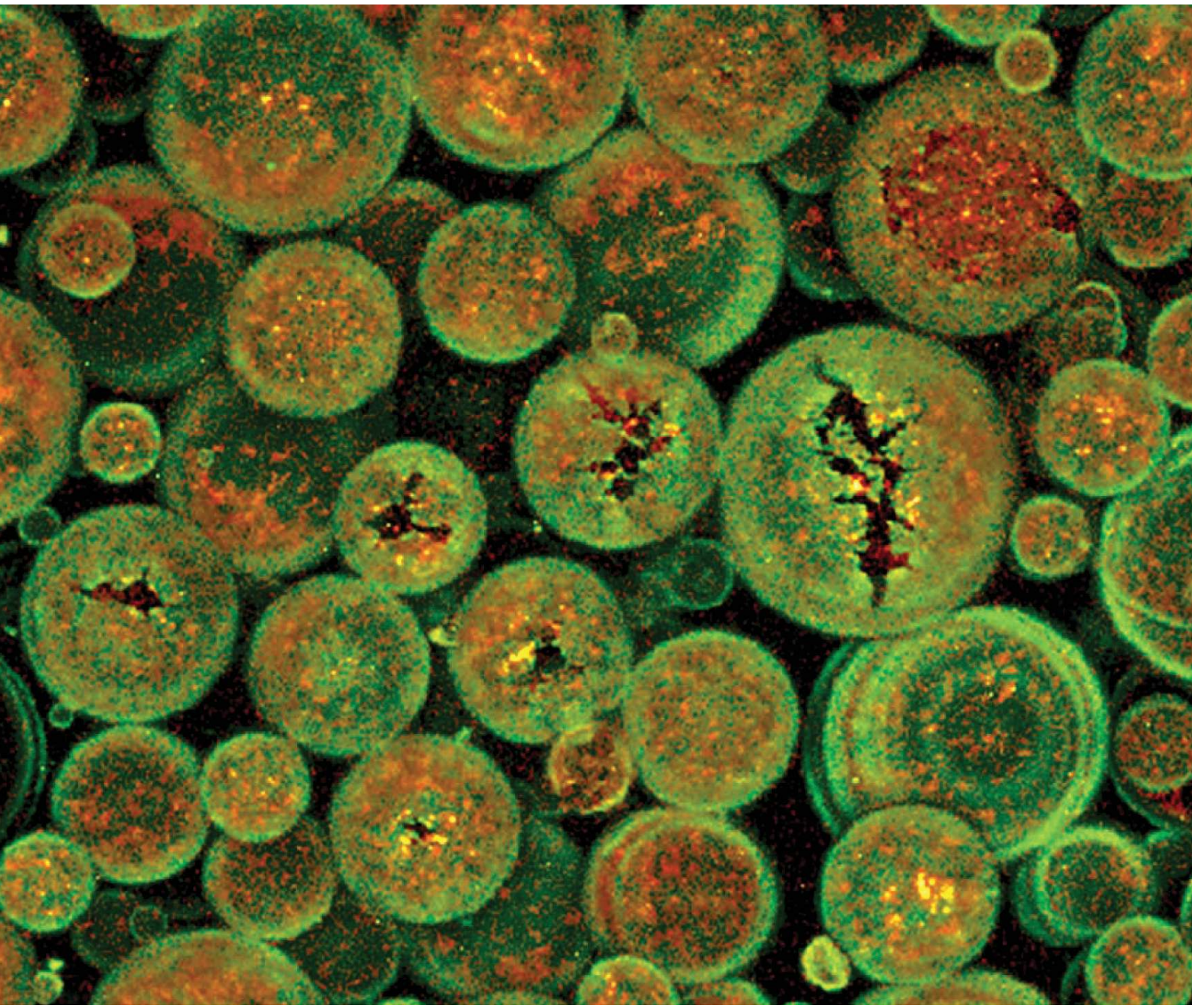

ISSN 1744-683X

REVIEW
Thomas Russell *et al.*
Self-assembly of nanoparticles at interfaces

PAPER
Patrick R. Unwin *et al.*
One-step formation of ultra-thin chemically functionalized redox-active Langmuir–Schaefer Nafion films

RSC Publishing

1744-683X(2007)3:10;1-I

Self-assembly of nanoparticles at interfaces

Alexander Böker,*[a] Jinbo He,[b] Todd Emrick*[b] and Thomas P. Russell*[b]

Received 2nd May 2007, Accepted 23rd July 2007
First published as an Advance Article on the web 4th September 2007
DOI: 10.1039/b706609k

Developments in the assembly of nanoparticles at liquid–liquid interfaces are reviewed where the assemblies can be controlled by tuning the size of the nanoparticles and the chemical characteristics of the ligands. Both synthetic and biological nanoparticles are discussed. By controlling the type of ligands, uniform and Janus-type nanoparticles can be produced where, at liquid–liquid interfaces, subsequent reactions of the ligands can be used to generate crosslinked sheets of nanoparticles at the interface that have applications including novel encapsulants, filtration devices with well-defined porosities, and controlled release materials. By controlling the size and volume fraction of the nanoparticles and the chemical nature of the ligands, nanoparticle–polymer composites can be generated where either enthalpy or entropy can be used to control the spatial distribution of the nanoparticles, thereby, producing auto-responsive materials that self-heal, self-corral assemblies of nanoparticles, or self-direct morphologies. Such systems hold great promise for generating novel optical, acoustic, electronic and magnetic materials.

1 Introduction

This review is concerned with the increasing use of liquid interfaces as templates for the self-assembly of colloidal particles.[1] In particular, besides micrometer-sized colloids, recently, nanoscopic particles with sizes down to a few nanometers were investigated. On one hand, the control of the structure formation processes at the nanometer level poses a challenging problem. On the other hand, the use of nanoparticles yields ample opportunities for the fabrication of nanostructured devices (*e.g.* nanoporous containers, or filtering devices). In addition to the use of classical oil/water emulsion systems, like the so-called Pickering emulsions, fluid interfaces such as those found in block copolymer nanostructures can be employed. Here, the nanoparticles impart specific functions to the nanostructures, such as magnetism or charge transport as required in magnetic data storage media or polymer-based photovoltaic devices, respectively.

1.1 Pickering emulsions

About a century ago, Pickering[2] and Ramsden[3] investigated paraffin–water emulsions, with solid particles such as iron oxide, silicon dioxide, barium sulfate and kaolin, and discovered that these micron-sized colloids generate a resistant film at the interface between the two immiscible phases, inhibiting the coalescence of the emulsion drops. These so-called Pickering emulsions are formed by the self-assembly of colloidal particles at fluid–fluid interfaces in two-phase liquid systems (Fig. 1). The desorption energy, which is directly related to the stability of emulsions depends on the particle size, particle–particle interaction and, of course, particle–water and particle–oil interactions.[4,5]

Approximately 70 years after Pickering's discovery, the behavior of the colloidal particles was described theoretically by Pieranski, who argued that the assembly of spherical particles at the oil/water (O/W) interface was determined by a decrease of the total free energy.[4] The placement of a single particle with an effective radius r, at the interface between an oil (O) und water (W) leads to a decrease of the initial interfacial energy E_0 to E_1 yielding an energy difference of ΔE_1:

$$E_0 - E_1 = \Delta E_1 = -\frac{\pi r^2}{\gamma_{O/W}} \cdot \left[\gamma_{O/W} - \left(\gamma_{P/W} - \gamma_{P/O}\right)\right]^2 \quad (1)$$

Here, the three contributions to the interfacial energy arise from the particle/oil interface ($\gamma_{P/O}$), the particle/water interface ($\gamma_{P/W}$), and the oil/water interface ($\gamma_{O/W}$). From eqn (1) it is evident that, for a given emulsion system (*i.e.* with fixed $\gamma_{P/O}$, $\gamma_{P/W}$, and $\gamma_{O/W}$), the stability of the particle assembly is determined by the square of the particle radius r. For microscopic particles the decrease in total free energy is much larger than thermal energy (a few k_BT) leading to an effective confinement of large colloids to the interface. Nanoscopic particles, however, are confined to the interface by an energy reduction comparable to thermal energy. Consequently,

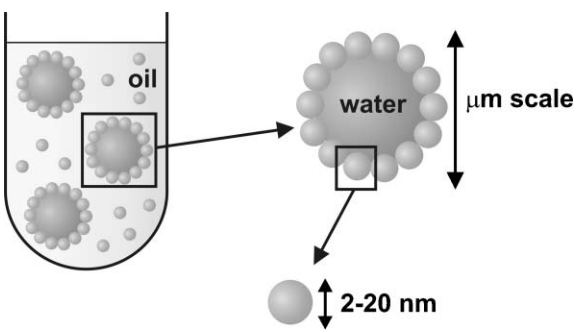

Fig. 1 Schematic of the self-assembly of solid nanoparticles at the oil–water interface.

[a]*Lehrstuhl für Physikalische Chemie II, Universität Bayreuth, Bayreuth, Germany 95440*
[b]*Department of Polymer Science & Engineering, University of Massachusetts, Amherst, MA, USA 01003*

nanoparticles are thus easily displaced from the interface, leading to a constant particle exchange at the interface, the rate of which depends on particle size. The thermally activated escape of small particles takes place more often than for larger ones, and for the equilibrium state of assembly, the total gain in free energy is smaller for smaller particles. Therefore, assemblies of larger nanoparticles are more stable. This size dependence allows the nanoparticle assembly to attain its equilibrium structure at the interface, whereas micrometer-size colloids may be trapped in a non-equilibrium state. Following these theoretical thoughts, various colloidal systems with particles of different size and surface chemistry (*e.g.* polystyrene latices, silica particles, *etc.*) have been described in the literature.[5–9] Moreover, the behavior of nanometer-size particles was investigated in detail due to their high potential for the construction of hierarchical and functional structures.[10–13]

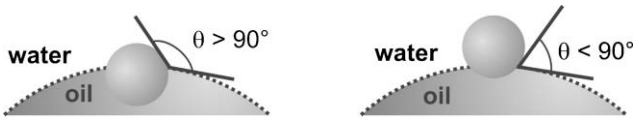

Fig. 2 Changes in wettability of solid particles at the oil/water interface at contact angles >90 and <90°.

In addition to the size of the nanoparticles, the interfacial tension and, therefore, the wettability of a particle surface, also dictates the desorption energy.[5] The wettability is described by the contact angle θ between the solid and the oil/water interface. Oil/water (O/W) or water/oil (W/O) emulsions are more stable depending on this contact angle. In general, the less wetting liquid becomes the dispersed phase. If the contact angle θ is lower than 90°, oil-in-water emulsions are more stable; at contact angles greater than 90°, water-in-oil emulsions are favored (Fig. 2).[14]

Alexander Böker

Alexander Böker is Lichtenberg-Professor for Colloid Chemistry at the University of Bayreuth, Germany. The main research interests of his group include guided self-assembly of block copolymer systems, hierarchical nanoparticle assemblies and the control of self-assembly processes via external fields. He is a member of the Bayreuth Center for Colloids and Interfaces (BZKG) and the Reimund Stadler Minerva Center for Mesoscale Macro-molecular Engineering.

Jinbo He

Jinbo He received his Bachelor's and Master's degrees in polymer chemistry and physics from Nanjing University in China. He is currently a graduate student in Prof. Russell's group in the Department of Polymer Science & Engineering at the University of Massachusetts in Amherst. His research interests are directing nanoparticle self-assembly at interfaces.

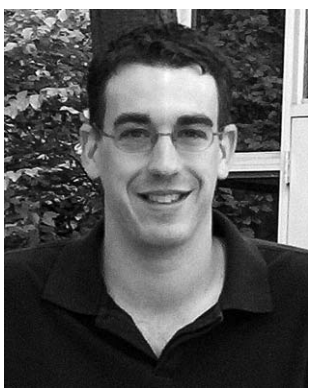

Todd Emrick

Todd Emrick is an Associate Professor of Polymer Science & Engineering at UMass Amherst, with research interests in organic, polymer, and nanoparticle synthesis. He completed a BS in chemistry at Juniata College (Huntingdon, PA) in 1992, and a PhD in organic chemistry at The University of Chicago in 1997 with Professor Philip Eaton. Following postdoctoral research with Jean M. J. Fréchet at the University of California Berkeley, he began his academic career at UMass Amherst in 2001. His group works on the synthesis of functionalized nanoparticles and polymers, including methods for tailoring these materials for interfacial segregation and reactivity at interfaces to give functional capsules and membranes for applications in controlled release and electronic materials.

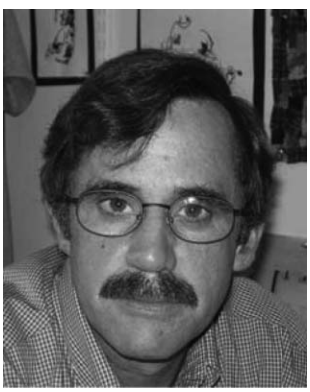

Thomas P. Russell

Thomas P. Russell, the Silvio O. Conte Distinguished Professor of Polymer Science and Engineering, received his PhD in 1979 in Polymer Science and Engineering from the University of Massachusetts Amherst. He was a Research Staff Member at the IBM Almadewn Research Center in San Jose, CA (1981–96) and became a Professor of Polymer Science and Engineering at the University of Massachuetts Amherst (1997). His research interests include the surface and interfacial properties of polymers, phase transitions in polymers, directed self-assembly processes, the use of polymers as scaffolds and templates for the generation of nanoscopic structures, the interfacial assembly of nanoparticles, and the influence of supercritical fluids on phase transitions and dynamics in polymer thin films. He is the Director of the Materials Research Science and Engineering Center on Polymers, an Associate Director of MassNanoTech, Director of the Multi-University Research Initiative on Nanoscopic Assembly of Biologically Active Materials, and an Associate Editor of Macromolecules. He is a fellow of the American Physical Society, the American Association for the Advancement of Science and the Neutron Scattering Society of America.

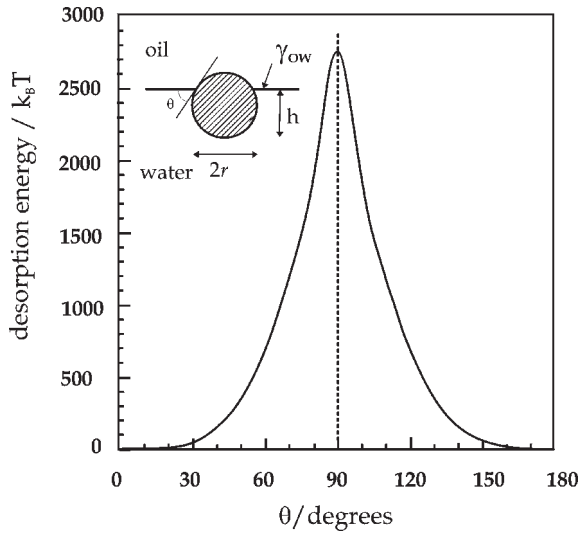

Fig. 3 Variation of the desorption energy of a spherical particle at a planar oil/water interface as a function of the contact angle θ. The depth of immersion into water is denoted as h, the particle radius is r = 10 nm, and the interfacial tension is $\gamma_{O/W}$ = 36 mN m^{-1}.[5] Reprinted with permission from *Langmuir*.[4] Copyright (2000) American Chemical Society.

The variation of the desorption energy with the contact angle θ is displayed in Fig. 3. Binks and Lumsdon investigated a toluene/water system with constant interfacial tension of 36 mN m^{-1}, with silica nanoparticles of constant radius of 10 nm, and various wettabilities, based on surface functionality.[5] At a contact angle of 90° a maximum in desorption energy is observed. Increasing or decreasing the contact angle, starting from the maximum stabilization at 90°, also decreases the stability of the emulsion. If the contact angle is between 0 and 20° or between 160 and 180°, the energy is 10 k_BT or less, which is on the order of magnitude of the desorption energy of conventional surfactants.[15]

So far, the stabilizing effect has only been described for particles with a homogeneous surface, *i.e.* a surface with homogeneous wettability. In section 2.2, we will give a brief introduction to the theoretically anticipated behavior of particles with a heterogeneous surface exhibiting heterogeneous wettability.

1.2 Nanoparticles as building blocks

Besides the basic interest in the parameters governing particle interfacial assembly, there is also considerable technological potential associated with the structures formed at liquid–liquid interfaces. For example, nanoparticles could serve as building blocks for capsules and membranes with nanoscopic pores for filtering or encapsulation and delivery purposes.

During the past years, several approaches for the design of nano- and microscopic capsules have been described in the literature. The electrostatic adsorption of polyelectrolytes[16–18] or particles[19] has also been investigated. Capsules have been successfully produced by polymerization in so-called mini-emulsions.[20] The most promising process so far uses a nanometer- to micrometer-size solid template of a water-insoluble substance, which is subsequently degraded to yield a hollow material.[21–23] These capsules swell in appropriate solvents and are filled by a diffusion controlled process from the surrounding phase. The drawbacks of this method are the broad pore size distribution, and the *ex situ* filling procedure during which only substances sufficiently small to pass the pores from the outside can be inserted into the capsule. Further experiments have focused on the use of liquid–liquid interfaces (*i.e.* water droplets dispersed in oil or a flat oil–water interface) as templates for the production of microporous capsules and membranes. Schüth, Fowler and others grew zeolite structures or silica spheres at such interfaces, but failed to generate structures with defined pore sizes and size distribution.[24–28]

Pore size control in microparticle colloidal assemblies were reported by Dinsmore *et al.*, using assembly of the particles at fluid interfaces, followed by sintering. The resulting interstices of the quasi-hexagonal array of particles gave pores in the range of several hundred nanometers.[29,30] Furthermore, Goedel *et al.* fabricated elastic, nanoporous membranes from silica–polyisoprene hybrid materials spread in a Langmuir trough. Crosslinking the nanoparticle–polyisoprene film by UV radiation, followed by dissolution of the silica particles, gave robust polymer membranes with pore sizes between 30 and 500 nm.[31–34]

It remains a challenge, though, to fabricate capsules and membranes with precisely controlled pore size and pore size distribution on the lower nanometer scale. Capsules with pores between 5 and 20 nm have been a long-standing goal for encapsulation and immunoisolation of cells for treatment of diabetes, cancer and other illnesses.[35–38] Upon implantation of living cells into a host, pores of this size protect the cells from the host's immune response, yet allow exchange of nutrients and secreted chemicals.[35–38] Existing approaches towards fabrication of immunoisolating capsules may result in a distribution of pore sizes too broad to be effective,[35] or may require laborious lithographic processing of one capsule at a time.[39]

A novel approach for the synthesis of such materials lies in the use of a nanoparticle toolkit that consists of particles with diameters ranging from 2 to 10 nm. The necessary toolkit is readily available due to the developments in nanoparticle synthesis (CdSe, Au, SiO_x, *etc.*) and surface functionalization methods using state of the art techniques.[40,41] So far, there are only a few publications dealing with the fluid directed self-assembly of nanoparticles. Many papers, however, describe particle self-assembly at solid interfaces. Korgel *et al.* for example created self-organized superstructures from 5 nm gold particles.[42,43] Analogous experiments using CdSe, CdTe and HgTe nanoparticles were described by Bawendi *et al.*[44] First studies on the nanoparticle self-assembly at curved (droplet) interfaces in Pickering emulsions were recently published by Lin *et al.*,[10,45,46] Mann *et al.*,[47] Dai *et al.*[48] and Möhwald and coworkers.[11–13]

2. Interfacial assembly of inorganic nanoparticles

2.1 Homogeneous nanoparticle assembly at fluid interfaces

The structure of CdSe nanoparticles (*i.e.*, quantum dots) segregated to the fluid interface has been investigated *ex situ*

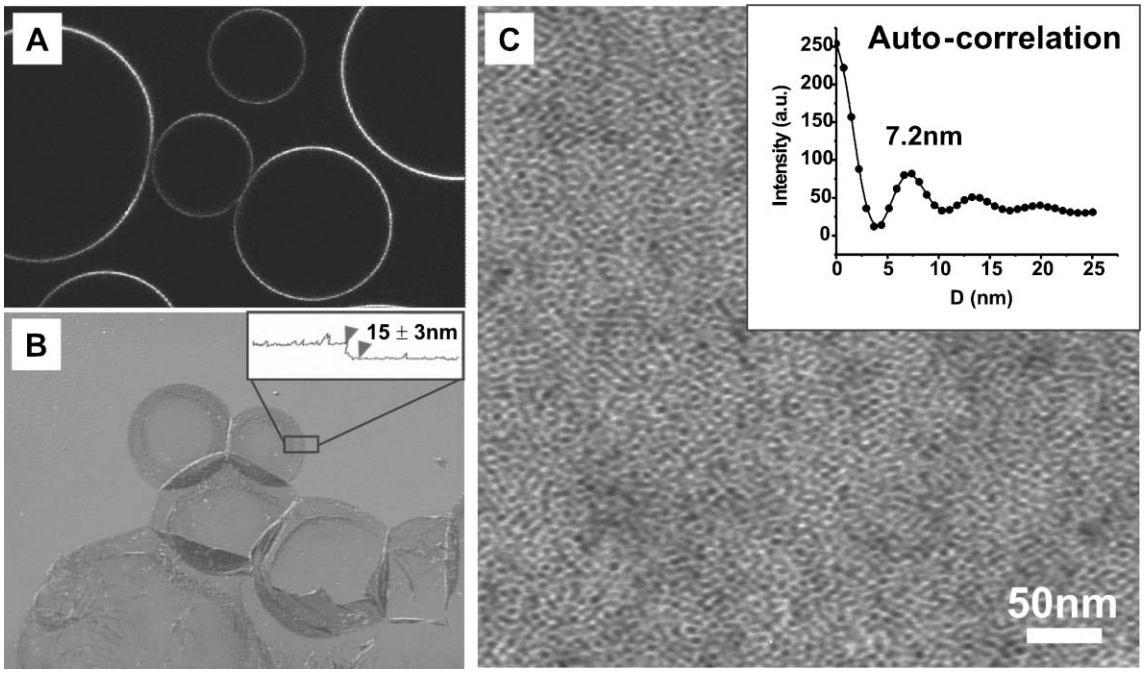

Fig. 4 (A) Fluorescence confocal microscope image of water droplets dispersed in toluene, covered with CdSe nanoparticles. (B) Differential interference contrast optical microscopy image of dried droplets on a silicon substrate. Inset: The AFM height section analysis shows two times the thickness of a monolayer. (C) TEM image of a dried droplet. Inset: Auto-correlation function of the TEM image revealing a mean particle distance of 7.2 nm which is in good agreement with the value expected for particles with 4.6 nm diameter and 0.8 nm hydrocarbon ligand.[45] Reprinted with permission from *Langmuir*.[45] Copyright (2005) American Chemical Society.

with scanning force microscopy (SFM) and transmission electron microscopy (TEM), and *in situ* with grazing-incidence small-angle X-ray scattering (GISAXS) methods. All results point to a monolayer of nanoparticles with liquid-like ordering at the interface (Fig. 4).[45]

In another approach, the interfacial diffusion of the nanoparticles was determined using two photobleaching methods: fluorescence loss induced by photobleaching (FLIP) and fluorescence recovery after photobleaching (FRAP). It was found that the lateral diffusion of the nanoparticles at the interface, as well as the diffusion normal to and from the interface, deviated by about four orders of magnitude from the values obtained in free solution.[45]

Moreover, a study using pendant drop tensiometry to follow the change in interfacial tension accompanied by simultaneous *ex situ* TEM measurements yielded insight into the mechanism of nanoparticle adsorption to the liquid interface. As can be inferred from the data in Fig. 5, different stages of adsorption can be distinguished. The TEM images in Fig. 6 show the mechanism of nanoparticle monolayer formation in detail. First, free nanoparticle diffusion to the interface occurs. Secondly, the particles pack closer and form clusters which grow to form a closely packed particle array, lowering the interfacial tension. Finally, thermally activated exchange between adsorbed and incoming particles is observed, leading to a tightly packed monolayer and only a slow decrease in interfacial tension at later times. These observations point to the formation of a nanoparticle monolayer by nucleation and growth. Furthermore, the relationship between the free diffusion and the diffusion for the late stage of adsorption, as calculated from the changes in interfacial tension, reveals an energy barrier at late stages that corresponds to the activation energy for a thermally triggered escape of nanoparticles from the interface. This is in good agreement with the observed packing behavior.

To fabricate mechanically stable capsules and membranes from the spherical nanoparticle assemblies, the adsorbed

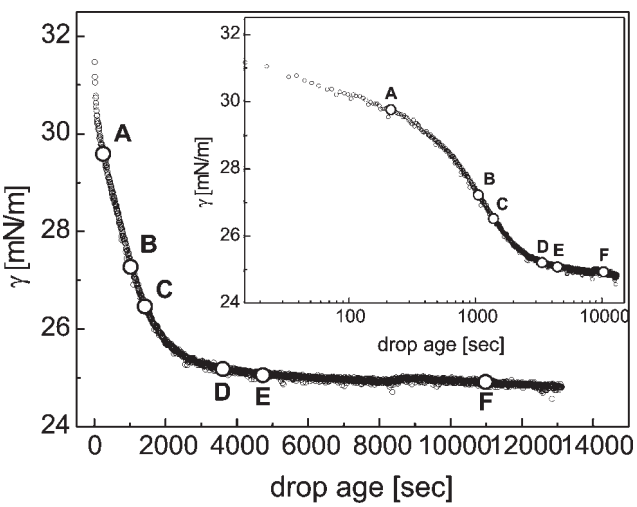

Fig. 5 Dynamic interfacial tension measurements of a toluene/water interface during adsorption of 6 nm CdSe nanoparticles to a pendant water drop in toluene ($c_{CdSe} = 1.58 \times 10^{-6}$ mol L^{-1}). The circles mark the time at which TEM samples shown in Fig. 6 were prepared. The inset depicts the data on a logarithmic time scale.

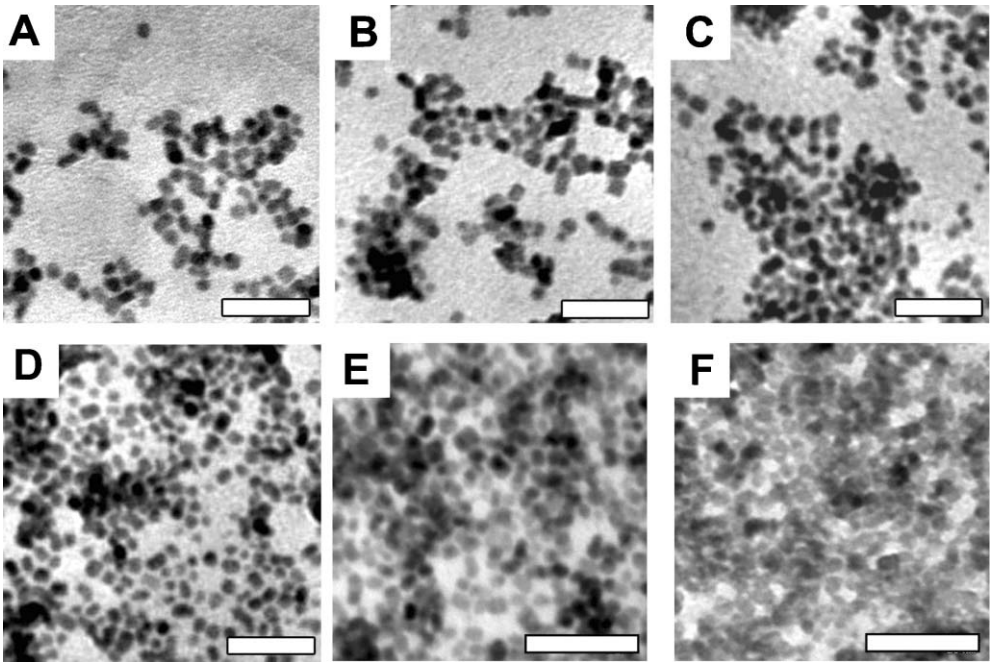

Fig. 6 Series of TEM images of 6 nm nanoparticle adsorption to the toluene/water interface at different adsorption times as marked in Fig. 5: A: 230 s, B: 1060 s, C: 1400 s, D: 3514 s, E: 4700 s, F: 10800 s. Structure formation *via* nucleation and growth of clusters can be seen. Scale bar: 40 nm.

particles need to be crosslinked at the interface. This can be done by the use of nanoparticles that are stabilized by reactive organic molecules. CdSe nanoparticles, stabilized by benzene vinyl ligands, segregated to the toluene/water interface, and were subsequently crosslinked using a water soluble radical initiator. This process yielded robust membranes that maintained their integrity even when removed from the interface (Fig. 7).[46]

Such crosslinked nanoparticle assemblies show high elasticity, extraordinary stability in water, and even serve as effective diffusion barriers for small molecule dyes. Using the process described above, a nanoparticle membrane has been generated in an Eppendorf tube at the toluene–water interface (Fig. 8). After removal of the organic phase and introduction of an aqueous Rhodamine B solution, within about 15 minutes, a well-defined diffusion of the dye across the membrane without any sign of turbulent mixing was observed (Fig. 8).[46]

Consequently, the use of functionalized ligands attached to the nanoparticles is shown to provide an effective means to stabilize the interfacial assembly by crosslinking. Moreover, the robust nanoparticle assembly proved to be as elastic and robust as expected for a nanometer thin sheet of polystyrene. This work can be seen as a proof-of-concept for the use of nanoparticles as building blocks for nanoporous membranes and capsules.

A drawback of the crosslinking strategy used initially for nanoparticle assemblies is the elevated temperature ($\sim$60 °C) necessary to initiate the radical crosslinking of the vinyl benzene ligands. Ligand systems have since been developed that allow crosslinking at room temperature. Ring opening metathesis polymerization (ROMP) was employed using a norbornene derivative as the ligand attached to CdSe/ZnS core-shell nanoparticles in combination with a water soluble PEGylated Grubbs catalyst (Fig. 9A/B). It was shown that these novel nanoparticles form stable assemblies at the toluene/water interface, and that, these assemblies could be crosslinked to yield well-defined CdSe/ZnS capsules (Fig. 9C).[49] Recently, Kotov *et al.* reported on the spontaneous formation of 2D

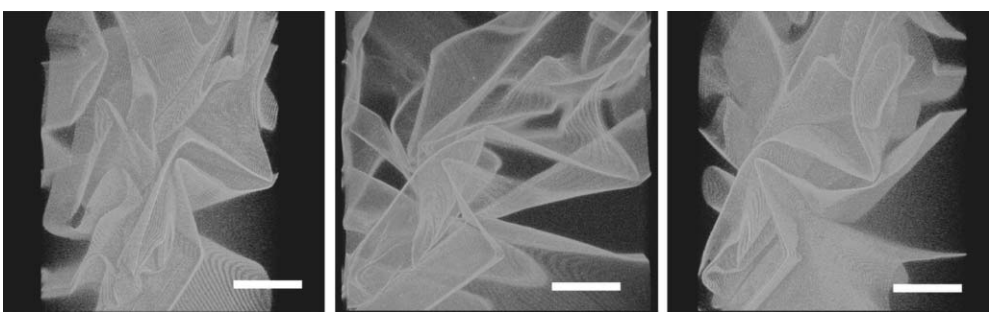

Fig. 7 Confocal microscope image from different viewing angles of a nanoparticle sheet prepared by crosslinking the functional ligands. The scale bars are 50 μm.[46] Reprinted with permission from *J. Am. Chem. Soc.*[46] Copyright (2003) American Chemical Society.

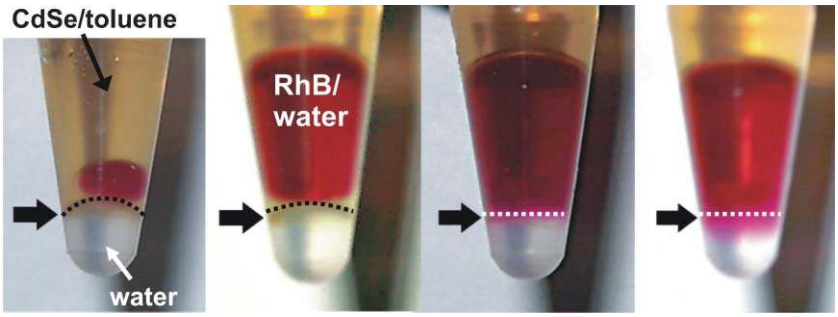

Fig. 8 Digital photographs of Rhodamine B dye (RhB, red solution) diffusing across a membrane of crosslinked nanoparticles (dotted line). The bold arrows point to the interface in each tube. The last two images represent a time frame of about 15 minutes.[46] Subsequent addition of water to the RhB/water droplet replaces the CdSe/toluene solution leading to a RhB/water–water interface separated by the nanoparticle membrane. Reprinted with permission from *J. Am. Chem. Soc*.[46] Copyright (2003) American Chemical Society.

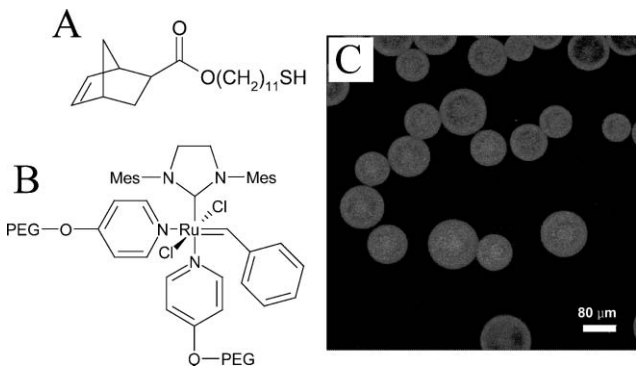

Fig. 9 (A) Structure of the norbornene ligand and (B) structure of PEGylated Grubbs-catalyst. (C) Confocal microscope image of nanoparticle capsules prepared by ROMP-crosslinking of the norbornene-functionalized CdSe/ZnS core-shell nanoparticles.[49] Reprinted with permission from *Adv. Mater*.[49] Copyright (2005) Wiley VCH.

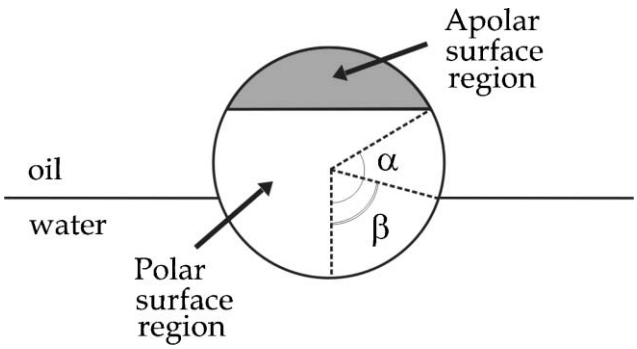

Fig. 10 Geometry of a Janus particle at the oil/water interface. The relative areas of the polar and apolar particle surface regions are parameterized by the angle α. β denotes the immersion angle of the particle at the oil/water interface.[52] Reprinted with permission from *Langmuir*.[52] Copyright (2001) American Chemical Society.

free-floating nanoparticle sheets from tetrahedral CdTe nanocrystals in solution.[50] Computer simulations revealed the interplay between the electrostatic interaction and anisotropic hydrophobic attraction between the nanoparticles to be crucial for the aggregation process. In addition, Tsukruk *et al.* generated free-standing polymer–nanoparticle composite films of only 20 nm thickness for sensor applications using a layer-by-layer (LbL) assembly technique.[51]

2.2 Janus-type nanoparticle assembly at fluid interfaces

The term Janus to describe nanoparticles is taken from the two-faced roman god. A Janus-particle is defined as having two distinctly different hemispherical or surface regions; polar and apolar regions are one example. Such a particle is characterized by two contact angles: θ_P as the contact angle of the polar region, and to θ_A as the contact angle of the apolar region (Fig. 10).

The ratio between the polar and apolar region can be changed where the angle α specifies the position of the surface boundary between both regions. Values of α of either 0° or 180° correspond to homogeneous particles, while a Janus particle in the original meaning would have a value of α of 90° due to the equal polar and apolar regions.[52]

The contact angles θ_A and θ_P correspond to the equilibrium angles given by Young's equation:

$$\cos\theta_A = \frac{\gamma_{A/W} - \gamma_{A/O}}{\gamma_{O/W}} \quad (2)$$

$$\cos\theta_P = \frac{\gamma_{P/W} - \gamma_{P/O}}{\gamma_{O/W}} \quad (3)$$

Here, $\gamma_{A/W}$, $\gamma_{A/O}$, $\gamma_{P/W}$, $\gamma_{P/O}$, and $\gamma_{O/W}$ refer to the interfacial energies of the apolar/water, apolar/oil, polar/water, polar/oil and oil/water interfaces, respectively. From the above mentioned properties it is obvious that Janus particles are surface active and amphiphilic, *i.e.* they combine the typical Pickering effect with the amphiphilicity of a classical surfactant. The question arises whether this can be used to their advantage with respect to the stabilization of oil/water emulsions. The amphiphilicity of a Janus particle can be changed by variation of the angle α or the difference between the two contact angles $\theta_A$and θ_P.

Fig. 11 shows the variation of the particle desorption energy in units of k_BT per particle with the average contact angle for Janus particles of different values of $\Delta\theta$, which is defined by $(\theta_P - \theta_A)/2$. For these calculations α, R and $\gamma_{O/W}$ are set to constant values of 90°, 10 nm and 36 mN m^{-1}, respectively.

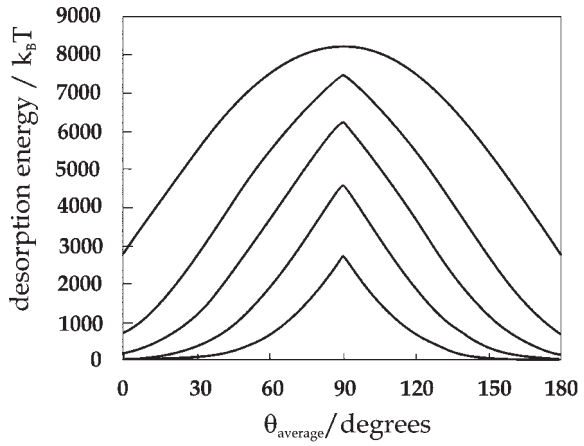

Fig. 11 Variation of the particle desorption energy with area weighted average contact angle for particles of radius 10 nm and α = 90°. The oil/water tension was set to 36 mN m^{-1}. In order increasing desorption energies, the curves refer to $\Delta\theta$ of 0 (the homogeneous particle case), 20, 40, 60 and 90° (bottom to top).[52] Reprinted with permission from *Langmuir*.[52] Copyright (2001) American Chemical Society.

The relative areas of the polar and apolar surface regions define the average contact angle ($\theta_{average}$) according to:[52]

$$\theta_{average} = \frac{\theta_A(1+\cos\alpha)+\theta_P(1-\cos\alpha)}{2} \quad (4)$$

Since α is set to 90°, this can be simplified to:

$$\theta_{average} = \frac{\theta_A+\theta_P}{2} \quad (5)$$

The particle amphiphilicity is tuned by changing $\Delta\theta$ which is defined as $(\theta_P - \theta_A)/2$. The five curves refer to $\Delta\theta$ of 0 (the homogeneous particle case), 20, 40, 60 and 90°. Particles having uniform wettability correspond to values of either α = 0° or 180° or for $\Delta\theta$ = 0 and, therefore, show zero amphiphilicity. The maximum amphiphilicity is expected in the case of α = 90° and $\Delta\theta$ = 90°. This corresponds to a Janus particle consisting of equivalent polar and apolar surface regions, in which the polar region is completely wetted by water and the apolar region is completely wetted by oil. In this case, the desorption energy is about three times larger than that for a comparable homogeneous particle. As discussed by Binks and Fletcher, amphiphilic Janus particles can exhibit an interfacial activity several times higher than simple homogeneous particles.[52] Janus particles combine the amphiphilic character of surfactants and the physical properties of nanoparticles, which opens new opportunities in emerging areas of nanotechnology and emulsions stabilization.

Recently, Perro *et al.*[53] reviewed the developments in the field of Janus particles during the last fifteen years, describing various strategies to obtain Janus-type particles using polymer precursors. One strategy is based on the self-assembly of ABC terpolymers in bulk[54,55] or in solution.[56] Another uses the electrostatic interactions of AB and CD diblock copolymers, which leads to inter-polyelectrolyte complexes.[57]A different synthetic concept is to obtain Janus particles made of inorganic materials, *e.g.* acorn-like particles made of PdS_x–Co_9S_8[58] or dumbbell-like CdS–FePt[59] and Ag–$CoFe_2O_3$.[60] Recently Duguet *et al.* showed the synthesis of an intermediate Janus particle composed of an inorganic part such as SiO_2 and an organic part consisting of polystyrene (PS) yielding dumbbell-like and snowman-like shapes.[61] Granick and co-workers successfully synthesized silica Janus colloid particles in large quantity at the liquid–liquid interface of molten wax and water.[62] Moreover, Cohen *et al.* produced Janus-type microcapsules *via* layer-by-layer assembly followed by stamping an additional polymer layer onto one side of the LbL-capsule.[63]

There have been considerable research efforts to obtain Janus particles, but none has realized Binks predictions,[52] as of yet. It is a challenging problem; especially for polymer based Janus structures, to clearly demonstrate the Janus character of the resulting objects. The advantage of inorganic Janus particles is that they have a well-defined structure and geometry, which can often be visualized by electron microscopy. Thus, the interfacial properties of Janus particles can be directly compared to their homogeneous analogues. Recently, Glaser *et al.*[64] prepared Janus particles (Fig. 12) consisting of a gold and an iron oxide part following a synthesis by Yu *et al.*[65] For the Janus particles, the mean diameter of the gold particle is around 4 nm while the diameter of iron oxide is about 10 nm resulting in an overall diameter of about 14 nm. (The diameters were determined by the image analysis program package *Image J*). The homogeneous nanoparticles show a slightly smaller diameter compared to the overall size of the Janus type: The gold nanoparticle diameter is about 10 nm and the iron oxide nanoparticle diameter is about 7 nm (Fig. 12). Subsequently, the particle amphiphilicity was tuned by ligand

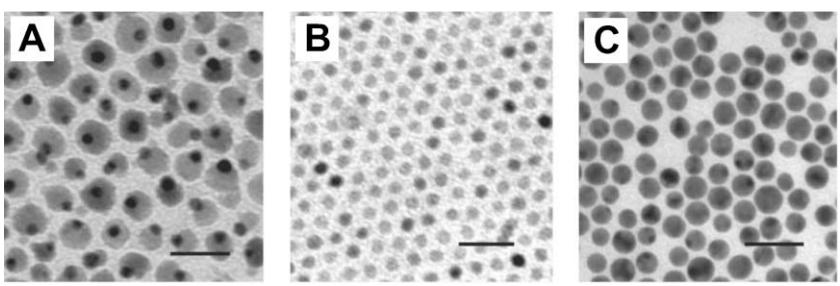

Fig. 12 TEM images of the nanoparticles: (A) Janus particles (consisting of gold (darker spheres) and iron oxide (brighter spheres)); (B) homogeneous iron oxide particles; (C) gold particles. Scale bars: 25 nm.[64] Reprinted with permission from *Langmuir*.[64] Copyright (2006) American Chemical Society.

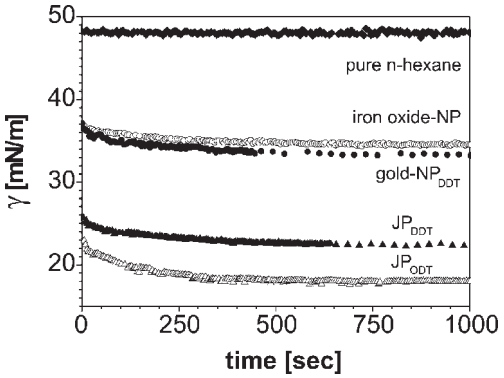

Fig. 13 Dynamic interfacial tension measurements of a hexane/water interface during adsorption of nanoparticles to a pendant water drop in hexane (for all particle types: $c = 1.2 \times 10^{-4}$ mmol L^{-1}). (NP: homogeneous nanoparticles; JP: Janus particles; the gold moieties were modified using dodecanethiol (DDT) or octadecanethiol (ODT)).[64] Reprinted with permission from *Langmuir*.[64] Copyright (2006) American Chemical Society.

exchange with dodecanethiol (DDT) or octadecanethiol (ODT) on the gold part and their interfacial activity was compared to those of the homogeneous gold and iron oxide particles using pendant drop tensiometry. The reduction in the interfacial energy supported the theoretical predictions of Binks and Fletcher (Fig. 13).[64]

2.3 Rod-type nanoparticle assembly at fluid interfaces

Recent synthetic advances in the preparation of inorganic nanoparticles provide many compositions of nanoscopic objects that are anisotropic in shape. Nanorods, for example, have attracted significant interest for the fabrication of functional materials with novel optical, electrical, and magnetic properties.[66–68] The liquid-crystal phase behavior of nanorods with different aspect ratios has been explored in the bulk.[69–71] However, simple methods to achieve a two-dimensional arrangement of nanorods with both orientational and positional ordering are still needed. Unlike isotropic colloidal particles, nanorods at interfaces are particularly interesting due to their shape. Such behavior has recently been investigated on the microscopic level[72,73] where a reorientation of ellipsoidal latex particles is seen at an air–water interface in response to an increase in the surface pressure.[73] Khanal and Zubarev found that at sufficiently low concentrations in dichloromethane, gold nanorod covered polystyrene ligands decorated the edge of water droplets (''breath figures'') in a head-to-tail fashion with nanorods parallel to the substrate during solvent evaporation.[74] Based on Pieranski's argument, the interfacial assembly is driven by a reduction of interfacial energy, for rod-like nanoparticles parallel or perpendicular to the fluid interface, the energy change for placing the nanorods at the interfaces is given by (Fig. 14)[73,75–77]

$$\Delta E_{//} = 2\pi RL[\pi(\gamma_{P/O} - \gamma_{P/W})] + \theta(\gamma_{P/W} - \gamma_{P/O}) + \gamma_{O/W}\sin\theta], \quad (6)$$

$$\text{where } \cos\theta = \frac{\gamma_{P/W} - \gamma_{P/O}}{\gamma_{O/W}} \quad (L \gg R)$$

$$\Delta E_{\perp} = (\gamma_{P/W} - \gamma_{O/W} - \gamma_{P/O})\,\pi R^2 + (\gamma_{P/W} - \gamma_{P/O})2\pi Rh \quad (7)$$

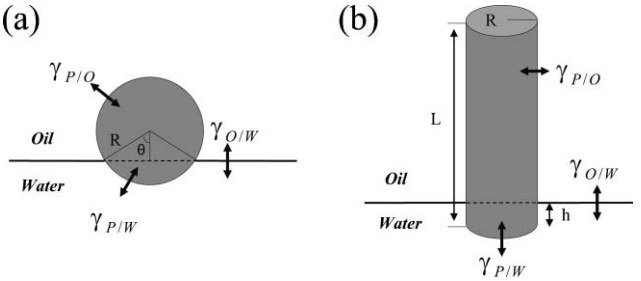

Fig. 14 Schematic of nanorods oriented parallel (a) and perpendicular (b) to the oil–water interface. R is the effective radius of the rods, L the effective length of the rods, γ the interfacial energy. P, O, W and θ represent the particle, oil, water and the contact angle of the particle at the interface, respectively. h is the depth of nanorods in the water phase when placed normal to the interface.[77] Reprinted with permission from *Small*.[77] Copyright (2007) Wiley VCH.

$\Delta E_{//}$ is defined as the energy change associated with nanorod assembly when the nanorods are parallel to the interface, and $\Delta E_{\perp}$ is the energy change when the nanorods are perpendicular to the interface. R and L are the effective radius and length of the rods, respectively, and γ is the interfacial energy. P, O, W and θ represent the particle, oil (toluene), water and the contact angle of the particle at the interface, respectively.[78] The penetration depth of the nanorods into the water phase, when assembled normal to the interface, is defined as h. These arguments predict that isolated nanorods are oriented parallel to the plane of the interface so as to maximize the interfacial coverage per particle and minimize the Helmholtz free energy of the system.

Tri-*n*-octylphosphine oxide (TOPO)-covered cadmium selenide (CdSe) nanorods were allowed to self-assemble at an oil/water interface formed by a drop of water at a solid substrate in contact with a toluene dispersion of the nanorods. The dispersion was rinsed away with pure toluene and the toluene was allowed to evaporate, leaving nanorods embedded on a water droplet in contact with air. The water evaporated subsequently and the in-plane compression, due to the decrease in the droplet surface area, caused the nanorods to exhibit a range of two-dimensional structures with different orientations. The structures observed span the range of the phase diagram, from a low-density smectic packing to a more-dense columnar ordering to a crystalline-like phase (Fig. 15). By controlling the interfacial energy between different liquids and nanoparticles, the aspect ratio of the nanorods, and their concentration, the lateral packing of the nanorods can be varied. Such control over self-assembly is key in designing hierarchically ordered structures that will open new opportunities in fabricating optical, acoustic, electronic, and magnetic materials and devices.[72,79–83]

2.4 Self-assembly of nanoparticle/polymer mixtures

2.4.1 Hierarchical nanoparticle assemblies formed by decorating breath figures. The formation of ''breath figures'', by the condensation of water droplets on the surface of a polymer solution, leads to a well-ordered hexagonal array of droplets. This assembly process can be coupled effectively with nanoparticle interfacial assembly at the polymer solution–water

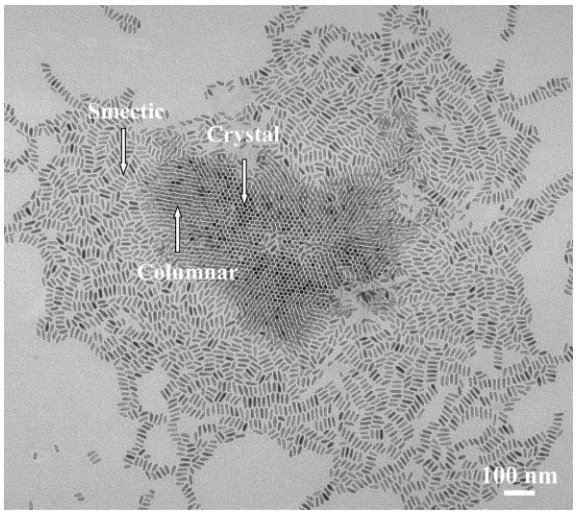

Fig. 15 TEM image of a CdSe nanorod-stabilized water droplet after drying on a carbon-coated copper grid.[77] Reprinted with permission from *Small*.[77] Copyright (2007) Wiley VCH.

droplet interface (Fig. 16). Complete evaporation of the organic solvent and water leads to a solid polymer film with water droplets embedded into the surface of the polymer. Upon evaporation of the water, the assembled nanoparticles are left deposited on the walls of the cavities, forming an array of decorated spherical cavities. It should be noted that it is the preference for the nanoparticles to assemble at the oil–water interface over the air–water interface that enables the preparation of such decorated breath figure structures. The structure of the nanoparticle assembly decorating the cavities can be probed *ex situ* using confocal microscopy and electron microscopy.[84]

This decoration process mimics the nanoparticle assembly in pure liquid systems. In this case, however, the final structure was frozen by solvent evaporation to yield "quasi *in situ*" insight into the structure formation process by allowing direct study of the nanoparticle assembly. Electron microscopy images showed that the particles formed a close packed monolayer at the interface between the water droplet and the nanoparticle/polymer solution. In addition, this combination of the two self-ordering processes has technological potential, as the interior of the well-ordered cavities is functionalized by the nanoparticle assemblies (Fig. 17). Subsequent *ex situ* ligand exchange of the CdSe nanoparticles after crosslinking of the polystyrene matrix may lead to further functionalization of the cavities for future applications as sensors or micro-reactors.[84]

2.4.2 Self-directed self-assembly of nanoparticle/copolymer composites. Incorporating nanoparticles into polymer matrices produces novel hybrid materials with special electrical, magnetic or optical properties. One approach is to directly evaporate or synthesize inorganic nanoparticles inside well-ordered block polymer templates. Cohen,[85] Sohn,[86,87] Möller[88] and coworkers have shown that polymer/nanoparticle composites can be generated by directly reducing the metal precursors inside block copolymer templates of different morphologies. Jaeger and Lopes demonstrated that by evaporating a series of

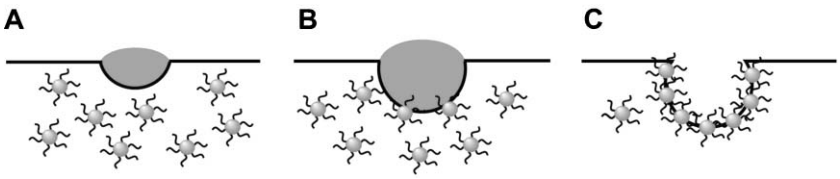

Fig. 16 A cross-sectional schematic of nanoparticle assembly at a water droplet–solution interface during "breath figure" formation. (A) A small water droplet condenses onto the nanoparticle/polystyrene solution and (B) sinks into the film while the particles segregate to the solution–water interface. (C) After the evaporation of the solvent and, subsequently, the water, the nanoparticles are trapped at the polymer–air interface, thereby functionalizing only the surface of the cavities.[84] Reprinted with permission from *Nat. Mater*.[84] Copyright (2004) Nature Publishing Group.

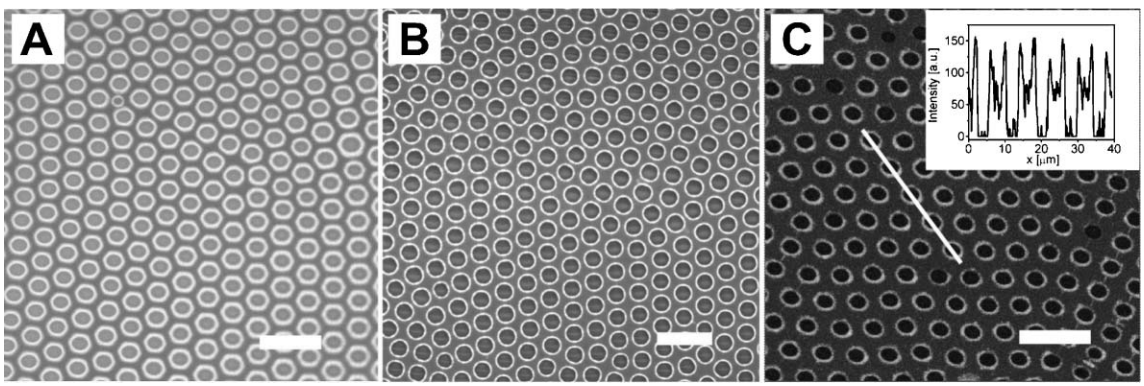

Fig. 17 (A) Breath figure pattern obtained with pure polystyrene. (B) Optical and (C) confocal fluorescence microscope images of different areas of a sample obtained from solvent casting a polymer film from a 7 wt% PS (76 k) solution in chloroform with 1 wt% 4 nm TOPO-covered CdSe nanoparticles at 80% relative humidity. Scale bars: 16 μm. The inset in C shows a fluorescence intensity scan along the line indicated.[84] Reprinted with permission from *Nat. Mater*.[84] Copyright (2004) Nature Publishing Group.

metal nanoparticles on polystyrene-block-poly(methyl methacrylate) templates, well-aligned metal wires could be obtained on the polystyrene domains after thermal treatment at 180 °C.[89] The disadvantages of these methods are lack of control of the size distributions of the nanoparticles, and lack of control of the position distributions of the nanoparticles inside the polymer matrices. Recently, Cheyne and Moffit demonstrated the formation of mesoscopic wires and cables *via* co-assembly of polystyrene-decorated CdSe nanoparticles and a polystyrene-block-poly (ethylene oxide) block copolymer at the water/air interface.[90]

Another approach is inspired by the recent theoretical arguments by Balazs and coworkers[91–93] that predict that block polymer/nanoparticle mixtures self-organize into hierarchically ordered structures dictated by the size, surface properties and volume fractions of the nanoparticles. Experimentally, Thomas and coworkers found that hydrocarbon-coated gold nanoparticles, with a diameter of 3.5 nm, segregated to the interface between the microdomains of poly(styrene-*b*-ethylene propylene) (PS-PEP) copolymer, while larger hydrocarbon-coated silica nanoparticles (21.5 nm in diameter) were located at the center of the PEP domains.[94] In the absence of specific enthalpic interactions between the two types of nanoparticles and the polymer matrix, the result suggests a profound influence of entropic contributions to the self-organization process. For large particles, the decrease in conformational entropy of the respective polymer subchains upon particle sequestration is dominant, whereas for smaller particles, the decrease in entropy is outweighed by the particle translational entropy.

Manipulating the location of nanoparticles in the materials can also be achieved by controlling the surface properties of the nanoparticles. By using enthalpic interactions, Kramer and coworkers found that gold nanoparticles covered with sufficient thiol-terminated polystyrene ligands are held inside the polystyrene microdomains in polystyrene-*b*-poly(2-vinylpiridine) (PS-*b*-P2VP) copolymers, while gold nanoparticles covered with both PS and P2VP ligands selectively segregate to the interfaces of PS and P2VP to minimize the interfacial energies.[95,96] A similar phenomenon is also observed by Composto and coworkers for immiscible polymer blends with silica nanoparticles present.[97] Subsequent reports demonstrated that controlling the ligand density on the surface of gold nanoparticles also greatly affects the nanoparticle positional distribution inside the PS microdomains. Strong enthalpic interaction between the gold nanoparticles and pyridine units in P2VP drive the nanoparticles with low PS ligand density to the interface of PS and P2VP, whereas at high PS ligand density, the blocking of enthalpic interaction results in a distribution of gold nanoparticles inside the PS microdomains.[98,99]

In the melt, block copolymer interfaces can be considered as "fluid" with dynamics much slower than for conventional liquids. However, the use of block copolymer interfaces provides an opportunity to study the nanoparticle assembly at fluid interfaces in more detail, since the polymer melt can be quenched at any stage of the assembly process. This allows the "quasi *in situ*" study of nanoparticle assembly at the block copolymer interfaces. Therefore, thin films from mixtures of a cylindrical polystyrene-*block*-poly (2-vinylpyridine), denoted as PS-*b*-P2VP, diblock copolymer with tri-*n*-octylphosphine oxide-(TOPO)-covered CdSe nanoparticles were prepared and investigated with SFM, TEM, and GISAXS after thermal annealing. Surprisingly, these composite materials are found to form hierarchically ordered structures *via* a cooperative self-organization. On the one hand, the cylindrical microdomains of the copolymer dictate the spatial distribution of the nanoparticles within the film. On the other hand, nanoparticles are found to segregate to the interfaces, mediating interfacial interactions and surface energies, resulting in an orientation of the cylindrical domains normal to the surface, even when the interactions of one of the blocks with the substrate are strongly attractive (Fig. 18). Thus, the synergy between two assembly processes produces unique structures, without the use of external fields, and opens a novel route to new self-directing, self-assembling architectures.[100]

To reveal the details of the cooperative self-organization of the PS-*b*-P2VP block copolymer/nanoparticle composites leading to the above described hierarchically ordered structures, the structure formation process was investigated with *in situ* GISAXS during thermal annealing. It was found that the orientation of the microdomains starts at the free surface and propagates into the film (Fig. 19), while the CdSe nanoparticles segregate to the P2VP phase, filling the cylinders from the top. To demonstrate the universality of this process, lamellar microdomain morphologies were used in addition to cylindrical ones. The results are shown in the SEM image in Fig. 20, where the microdomains of a lamellar PS-*b*-P2VP block copolymer oriented perpendicular to the substrate can

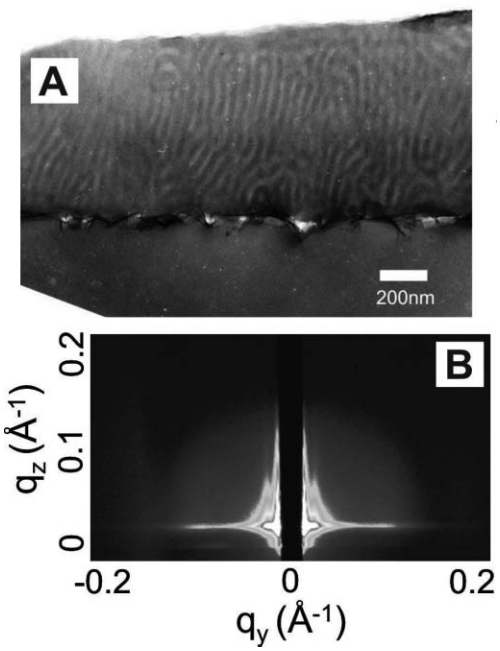

Fig. 18 (A) TEM image of cross section of a PS-*b*-P2VP block copolymer/CdSe nanoparticle film after annealing at 170 °C for 2 days. (B) Data from GISAXS measurements: of the same film at incident angle of 0.09° with a penetration depth of 61 Å.[100] Reprinted with permission from *Nature*.[100] Copyright (2005) Nature Publishing Group.

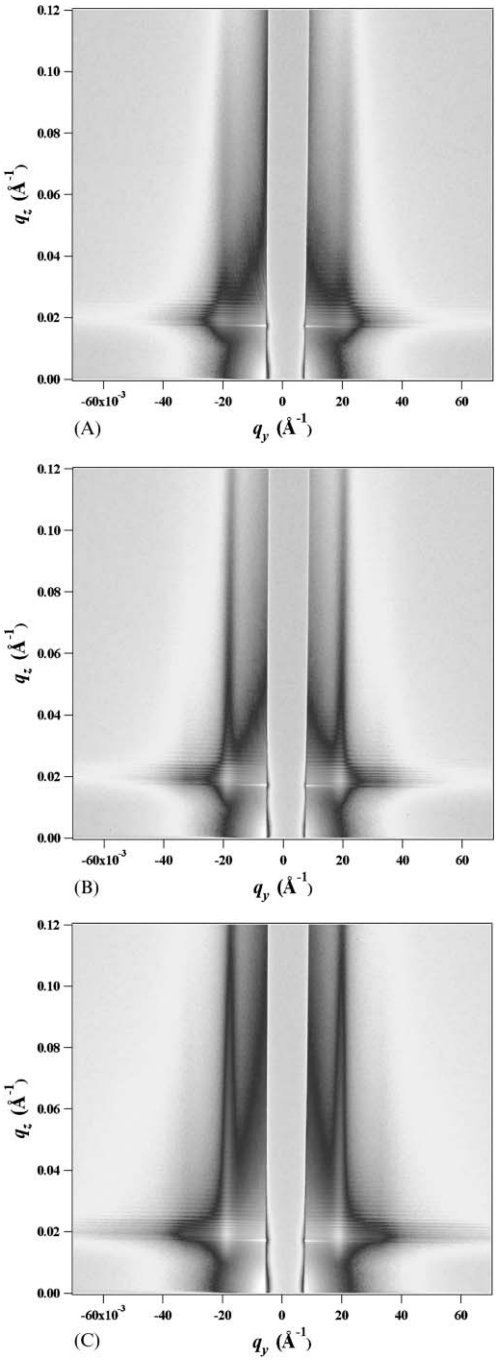

Fig. 19 Series of *in situ* GISAXS images of a cylindrical nanoparticle-doped PS-*b*-P2VP film during thermal annealing at 180 °C: A: after spin coating (0 h), B: 4 h, C: 14 h.[101] Reprinted with permission from *Adv. Mater*.[101] Copyright (2007) Wiley VCH.

be seen. The inset depicts the decoration of the lamellae with CdSe nanoparticles (bright spots).

2.4.3 Crack-healing based on nanoparticle/polymer composites. Multilayer composites that combine ductile polymers with brittle films constitute vital components for optical communications, microelectronics and bio-engineering applications. However, crack formation is a critical problem in these materials. Thus, designing layered systems that can

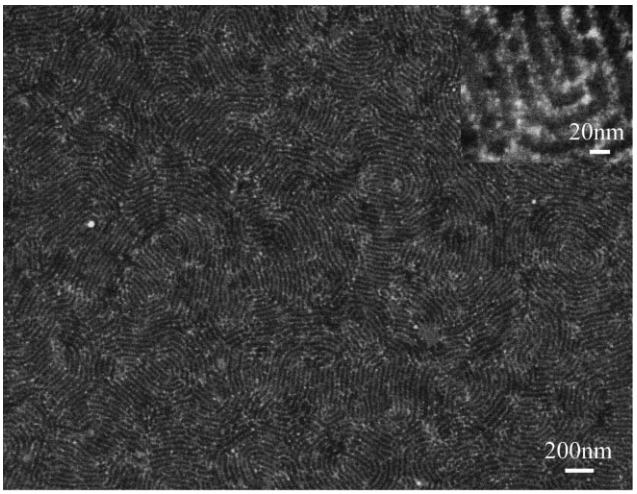

Fig. 20 High resolution SEM image of the lamellar PS-*b*-P2VP (25.5 K–23.5 K)/CdSe nanoparticle composite thin film after annealing in $CHCl_3$ for 1 day, without staining. The image is taken at 1 kV acceleration voltage.[101] Reprinted with permission from *Adv. Mater*.[101] Copyright (2007) Wiley VCH.

respond to environmental changes and undergo self-healing is particularly important for a range of technologies. Computational studies on filled homopolymers near a surface containing a notch or crack showed that the polymer melt induced an entropic "depletion attraction" between the particles and the surface that drove a fraction of the nanoparticles into the defect.[102,103] These predictions were recently confirmed experimentally on a multilayer comprised of PEGylated CdSe nanoparticles dispersed in poly(methyl methacrylate) (PMMA) in contact with a brittle silicon oxide layer.[104] Heating the bilayer above the glass transition temperature of the polymer induced cracking of the SiOx layer and nanoparticles that were comparable in size to the radius of gyration of the PMMA migrated into the crack, as shown in the fluorescence optical micrograph in Fig. 21.[105] However, for smaller nanoparticles, this behavior was not observed, because the polymer can easily accommodate the nanoparticles without a substantial entropic penalty.[104] Similar entropic interactions were operative in polystyrene (PS)–functionalized CdSe dispersed in PS examined by Crosby and co-workers, in which nanoparticles were found to segregate to the tip of a crack and modify the crazing characteristics of a glassy polymer.[106] These findings open a convenient route for designing self-healing systems.

3. Interfacial assembly of biological nanoparticles

3.1 Biological nanoparticles

Compared to inorganic colloidal or nanoscopic particles, bionanoparticles have unique advantages, including a truly monodisperse size-distribution and a range of versatile surface functionalities available for modification on the protein shell. Recently, bionanoparticles such as, cowpea chlorotic mottle virus (CCMV); cowpea mosaic virus (CPMV); turnip yellow mosaic virus (TYMV); tobacco mosaic virus (TMV), M13 bacteriophage and ferritin, have aroused great interest in the

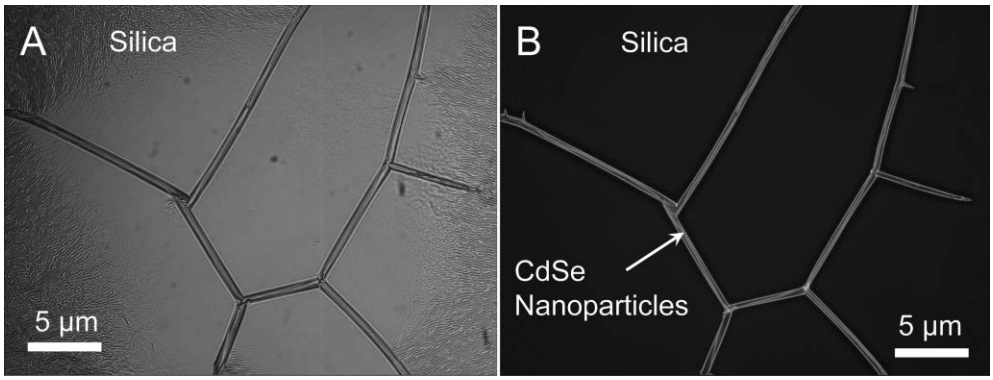

Fig. 21 (A) A reflection optical micrograph of a thin film of a mixture of 6-nm PEGylated CdSe nanoparticles in poly(methyl methacrylate) that was spin-coated onto a silicon wafer. A 0.1-mm layer of silicon oxide was evaporated onto the nanoparticle composite and the trilayer was heated to 160 °C for 4 hours. The difference in the thermal expansion coefficients of silicon oxide and the PMMA composite produced the cracks observed. (B) The same film viewed with a fluorescence microscope, in which the segregation of the CdSe nanoparticles to the cracks is highlighted by the fluorescence of the nanoparticle.[105] Reprinted with permission from *Science*.[105] Copyright (2006) Science.

field of self-assembly. The use of bionanoparticles as scaffolds or building blocks has been explored for synthesis of magnetic and semiconducting materials, based on the inherent ability of these particles to self-assemble and the opportunities to modify the protein surface by chemical or genetic methods.[107–129] In the past fifteen years, numerous studies have focused on generating ordered two-dimensional arrays of protein particles for applications in nanotechnology or electron crystallography.[130–136] By spreading and adsorbing proteins on surfaces or at interfaces, Nagayama and co-workers have assembled different 2D protein crystals at the interface of air–water,[134,136] mercury–water[137–139] and hexane–water,[140] based on electrostatic interactions. However, simple and fast routes to direct and assemble bionanoparticles into 2D or 3D constructs with hierarchical ordering are still needed. The Self-assembly of bionanoparticles at liquid–liquid interfaces provide a good example of this approach.

Here, we focus on cowpea mosaic virus (CPMV) and horse spleen ferritin (HSF). The molecular structures, molecular weights, and dimensions are shown in Fig. 22 and Table 1. These systems exhibit a wide range of properties (size, shape, biology and chemistry), and process characteristics

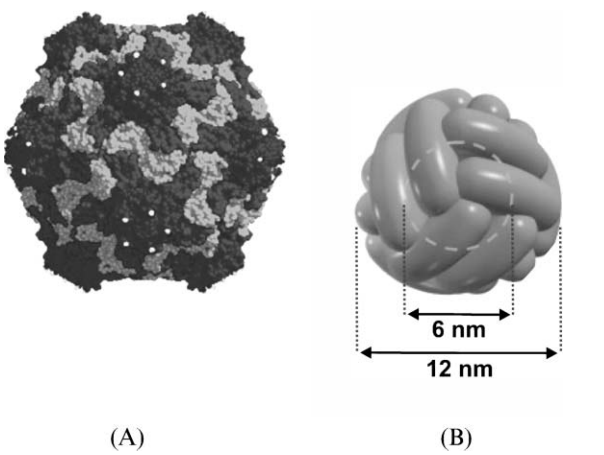

Fig. 22 Molecular structure of the cowpea mosaic virus (CPMV)[144] and horse spleen ferritin (HSF).[145,146]

(availability of high-yield expression vectors and isolation and purification protocols).[141–144]

Cowpea mosaic virus measures approximately 30 nm in diameter and can be isolated from infected plants in yields of 1–2 g kg^{-1} of leaves.[143] CPMV is icosahedral in shape and noninfective toward mammals, and, thus, constitutes no biological hazard. The CPMV capsid is very stable, able to withstand 65 °C, and tolerate a pH range from 3 to 10. The capsid is also stable to some organic solvents, up to 20% DMSO or dioxane,[147] which is an important prerequisite for possible modification and crosslinking reactions at interfaces. Its X-ray structure has been determined to 2.8 Å resolution,[144] showing a capsid with an asymmetric unit containing three β-sandwich folds formed by two polypeptides (Fig. 23A). Sixty copies of the two-protein asymmetric unit (composed of a "small" subunit, the A domain, and a "large" subunit, the B + C domains, Fig. 23B) are assembled in an icosahedral pattern around the single-stranded viral genomic RNA to form the virus particle. CPMV is a particularly attractive nanoparticle because the capsid surface chemistry of CPMV has been studied extensively.[110,117,148,149] The wild type CPMV shows at least one easily accessible and reactive lysine side chain per asymmetric unit (Fig. 23C), which can serve as an anchoring group for crosslinking reactions.[148] A detailed study on lysine reactivities is given by Chatterji *et al.*[150]

In addition, the insertion of exogenous peptides or the mutation of existing residues for the purposes of engineering novel function is well established; such altered viruses are known as *chimeras*. Their production is made straightforward by the development of an infectious DNA clone of CPMV,[144,151–153] which can be used to produce virus by simply rubbing a small amount on a leaf of the target plant. It

Table 1 Characteristics of the cowpea mosaic virus (CPMV)[144] and horse spleen ferritin (HSF).[145,146]

	CPMV	HSF
Diameter/nm	28–32	12
M_w (capsid)/D	3.9×10^6	4.4×10^5
M_w (subunit)/D	24k & 42k	1.85×10^4
Symmetry	Icosahedral ($T = 1$)	Octahedral

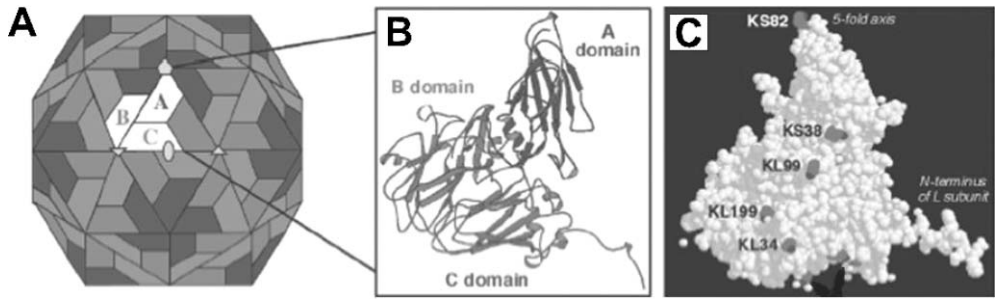

Fig. 23 Structural model of wild type cowpea mosaic virus (CPMV): (A) Subunit organization, (B) subunit ribbon diagram, and (C) space-filling model of the coat protein. The latter shows the exterior surface of the asymmetric unit with lysine side chain carbon and nitrogen atoms. Two lysine residues of the small subunit (S82, S38) appear to be exposed to solvent, whereas three in the large subunit (L99, L199, and L34) are also visible.[148] Reprinted with permission from *Chemistry & Biology*.[148] Copyright (2002) Elsevier LTD.

has been shown that such a modification leads to multiple reactive sites (including the one native reactive lysine[148] and two newly inserted reactive cysteines)[149] which can be addressed regioselectively, *i.e.* functional groups can be anchored at pre-designed positions on the viral surface.

Mono-maleimide functionalized gold nanoparticles, as well as pure gold particles, have been employed to address the newly inserted cysteines. Cryo-electron microscopy analysis with 3D reconstruction of the product showed the densities of gold, which were superimposed on the atomic model of CPMV showing that the gold is attached at the site of cysteine insertion.[147,154] Therefore, CPMV can be readily decorated with nanoparticles *via* maleimide chemistry.

Ferritins are iron storage protein cages belonging to the Class II diiron-carboxylate proteins[145]. The tertiary and quaternary structure of ferritins is highly conserved. All ferritins are composed of 24 subunits arranged in octahedral symmetry, which self assemble to form a 12 nm diameter cage with a 7.5–8 nm diameter cavity, the so-called Apoferritin (440 kDa).[155] About 4000 iron atoms are stored in the central core of ferritins as iron(III) oxyhydroxide, mainly ferrihydrite ($5Fe_2O_3{\cdot}9H_2O$).[146] Ferritins are remarkably stable particles, withstanding 70 °C and tolerating a pH range between 2 and 10.[156] Several studies have demonstrated that ferritin can be used as a nanoreactor for the formation of inorganic nanocrystals.[157,158] Self-assembly of ferritin on a solid surface or liquid–air interface can afford well-defined 2D structures.[130,132,133,159] Furthermore, it is possible to detect the direct electron transfer from ferritin to gold electrodes.[156,160] As shown in Fig. 24, the exterior surface of HSF can be chemically modified with a variety of functionalities similar to CPMV.

For both CPMV and horse spleen ferritin (HSF), there are more than two orthogonal reactive sites per subunit that can be addressed chemoselectively.[147–149,162–165] Therefore, the bionanoparticles described here have potential as highly functional, well-defined and monodisperse building blocks for 2D and 3D constructs (*e.g.* membranes and capsules).

3.2 Self-assembly and cross-linking of bionanoparticles at liquid–liquid interfaces

In addition to the self-assembly of inorganic nanoparticles, Pickering emulsions can be prepared using bionanoparticles (BNP) such as those described above. Horse spleen ferritin

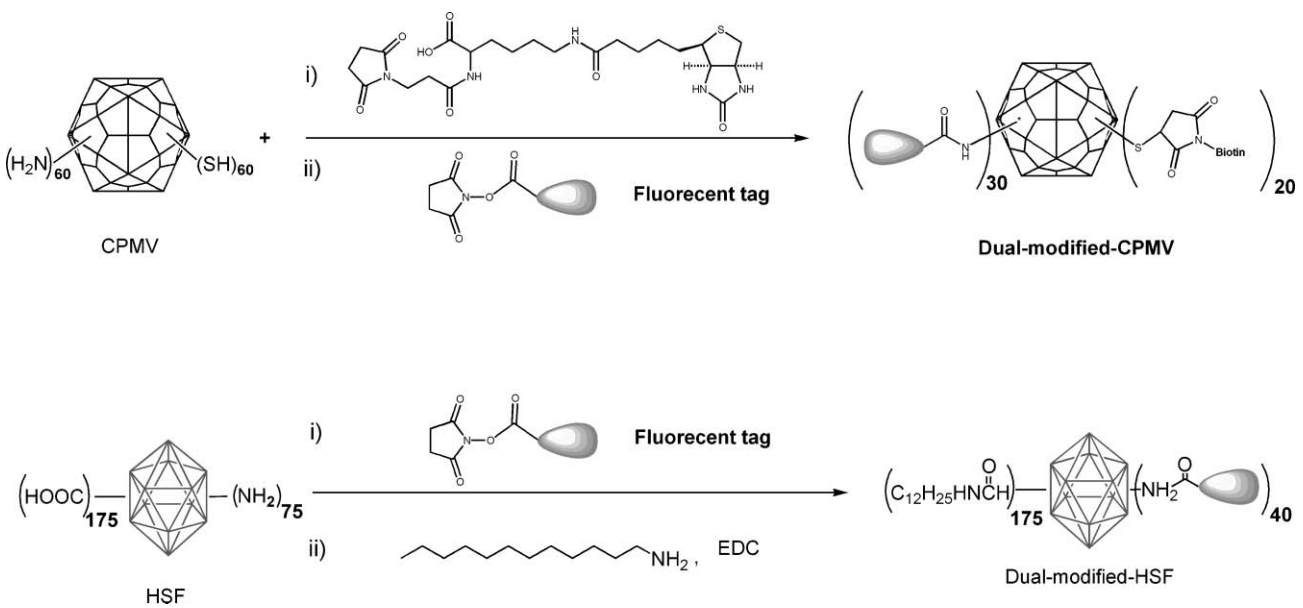

Fig. 24 Chemoselective labeling of cow pea mosaic virus (CPMV) and horse spleen ferritin (HSF).[148,161,162]

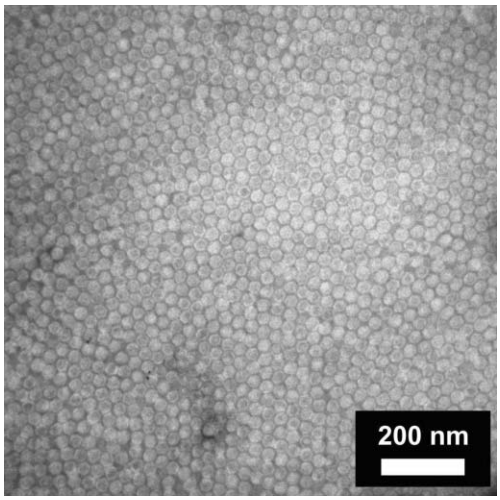

Fig. 25 Transmission electron micrograph of densely packed CPMV assembly at the oil/water interface stained with uranyl acetate (2 wt% in water).

(HSF) and CPMV can be self-assembled at the perfluorodecalin/water interface, then crosslinked with glutaraldehyde, taking advantage of surface available lysine residues. The assembly process, the presence of liquid interfaces, and the subsequent reactions on the particles at the interface all proceed without disruption of the virus particle integrity, as can be seen from a TEM image obtained from a CPMV membrane (Fig. 25).

Perfluorodecalin droplets with diameters from 10 to 100 microns were obtained by adding perfluorodecalin into a dispersion of fluorescently labeled CPMV or HSF in buffer solution, followed by vigorous shaking. The particles, dispersed in aqueous buffer initially, assembled at the perfluorodecalin–water interface, and stabilized the dispersion of the water droplets, forming Pickering emulsions.[161]

Fig. 26A shows a fluorescence confocal microscope image of a 3D reconstruction of wild-type CPMV coated perfluorodecalin droplets after crosslinking with glutaraldehyde and removal of excess particles in the buffer phase by washing with water. Complete removal of the water and perfluorodecalin disrupts the crosslinked virus shell around the oil phase. Upon rehydration with buffer solution, crumpled shells are observed as shown in Fig. 26B. Fig. 26C depicts a spherical cap generated by the assembly and subsequent crosslinking of CPMV around a perfluorodecalin droplet that was placed on a glass slide. After complete drying and washing with buffer and water, the cap folded backwards, revealing distinct wrinkles on the surface. To determine the thickness of the crosslinked virus particle assembly, SFM images were recorded at the

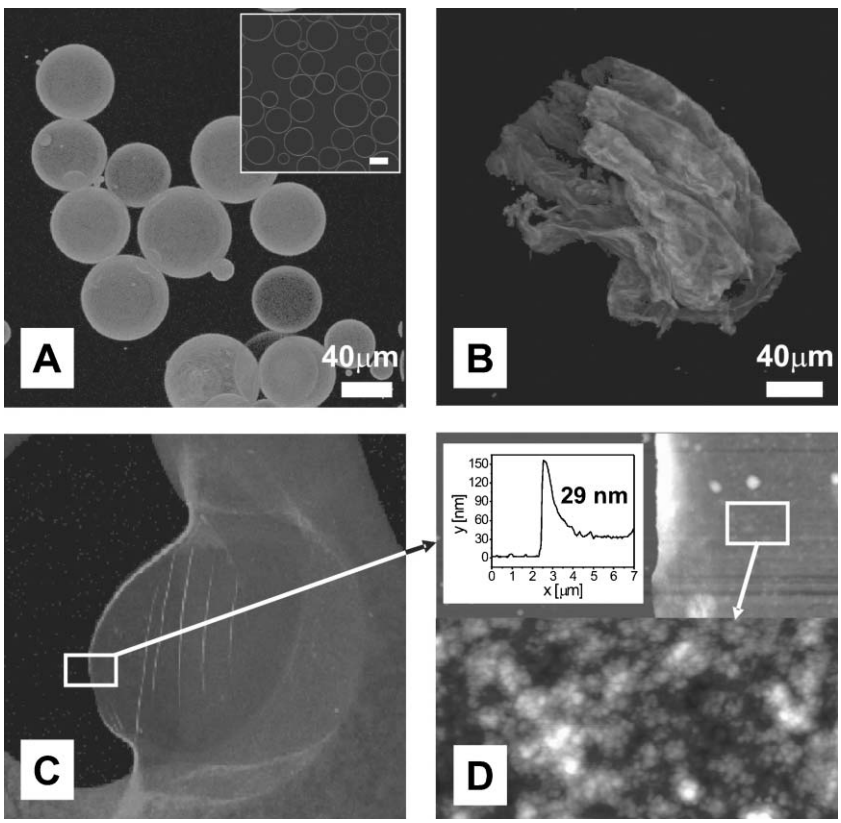

Fig. 26 Confocal fluorescence microscope images of CPMV assembly after crosslinking with glutaraldehyde. (A) 3D reconstruction of virus-coated perfluorodecalin droplets in water (inset: cross-sectional view). Excess particles have been removed by successive washing with water. (B) Crumpled droplet after complete drying and rehydration with water. (C) Capsule cap after complete drying. The white box indicates the area at which the SFM scan in (D) was taken. The lower part of (D) shows the height profile on top of the collapsed capsule (image width: 2 μm, *z*-range 30 nm).[161] Reprinted with permission from *Angew. Chem. Int. Ed.*[161] Copyright (2005) Wiley VCH.

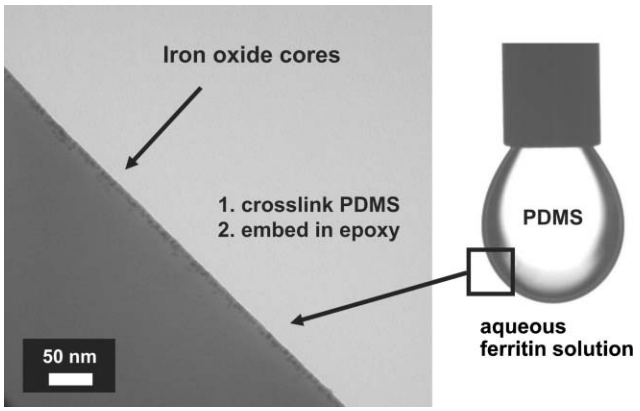

Fig. 27 Cross sectional transmission electron micrograph of ferritin assembly at silicone oil–water interface (iron core size: 6 nm).

edge of the back folded cap. The white box in Fig. 26C indicates the spot where the SFM image in Fig. 26D was taken. Cross-sectional analysis yielded a step height of 29 $\pm$ 2 nm. This is consistent with a monolayer formed by virus particles of 28–32 nm in diameter. Small angle neutron scattering (SANS) showed a close packed single layer of CPMV particle assembled at the interface.

To further demonstrate the degree of control over bionanoparticle assembly at various interfaces, pendant drop tensiometry was used to study ferritin particle assemblies at the interface between a crosslinkable PDMS precursor and the aqueous nanoparticle solution. After complete assembly, the precursor was crosslinked to give solid PDMS, removed from the solution, washed to remove non-adsorbed particles, and finally embedded into an epoxy resin and microtomed. The resulting TEM image (Fig. 27) shows the iron cores of the ferritin particles. This reveals the formation of a well defined monolayer of ferritin nanoparticles at the liquid interface.

Qualitative experiments were also performed to evaluate the function of self-assembled bionanoparticles as membranes. After monolayer adsorption at the chloroform–water interface, the CPMV fluid–fluid assembly was crosslinked with glutaraldehyde. Finally, most of the upper aqueous buffer solution was replaced with an ethanol solution of Sudan Red 7B, allowing for diffusion of the dye from the ethanol to the chloroform phase. The CPMV membrane, however, remained intact and prohibited turbulent mixing of the dye and water phase. Therefore, a clear diffusion front could be observed (Fig. 28).

4. Conclusion

The interfacial self-assembly of nanoparticles has been discussed and examples are highlighted above. For liquid–liquid interfaces, reduction in the interfacial energy is the dominated driving force, which is essentially enthalpically driven. The assembly can be manipulated by tuning the particle size or surface properties, including the special case of Janus particles. Anisotropic nanoparticles behave differently at the interfaces due to their shape. Different orientation and packing structures of nanorods at the liquid–liquid interface can be generated by controlling the aspect ratio, surface properties, concentration, and solvent evaporation rates. Bionanoparticles provide unique building blocks for assembly at interfaces due to their genetic nature. Uniform sizes, and versatile functionalities on the protein shells provide unique opportunities in filtration, encapsulation, and cell adhesion. For polymer based interfaces, depending on the surface properties and sizes of the nanoparticles, the system can be either enthalpically or entropically driven. The self-assembly of nanoparticles can have synergistic interactions with another self-organizing system to yield hierarchical structures or heal defects in the composites. Given the wide range of synthetic methods for well-defined nanoparticles of many types, the self-assembly of nanoparticles into hierarchically ordered structures, using interfacial interactions to advantage, represents a rich new area for fabricating optical, acoustic, electronic, and magnetic materials.

Acknowledgements

This work was supported by the US Department of Energy, Office of Basic Energy Science (DE-FG02-96ER45612 and DE-FG02-04ER46126), the Army Research laboratory through the MURI program (W911NF-04-1-0191), the NSF-supported MRSEC at the University of Massachusetts Amherst (DMR-0213695), an NSF CAREER Award (CHE-0239486) and the NSF-supported CRC (CHE-0404575). AB thanks Unilever Corporate Research, the German Science Foundation (SFB 481, TP B10) and the VolkswagenStiftung (Lichtenberg-Programm) for financial support and Michaela Hoffmann, Günther Jutz and Sergej Kutuzov for their contributions.

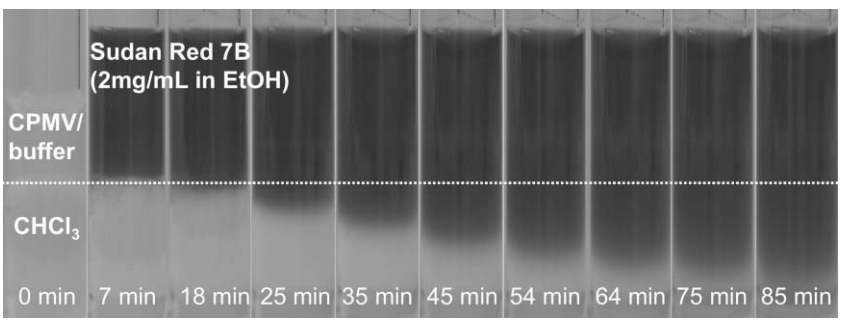

Fig. 28 Dye diffusion through a CPMV-based membrane crosslinked with glutaraldehyde. The dotted line shows the position of the membrane.

References

1 B. P. Binks and T. S. Horozov, *Colloidal Particles at Liquid Interfaces*, Cambridge University Press, Cambridge, 2006.
2 S. U. Pickering, *J. Chem. Soc., Trans.*, 1907, **91**, 2001–2021.
3 W. Ramsden, *Proc. R. Soc. London, Ser. A*, 1903, **72**, 156–164.
4 P. Pieranski, *Phys. Rev. Lett.*, 1980, **45**, 569–572.
5 B. P. Binks and S. O. Lumsdon, *Langmuir*, 2000, **16**, 8622–8631.
6 B. P. Binks and S. O. Lumsdon, *Langmuir*, 2001, **17**, 4540–4547.
7 B. P. Binks and C. P. Whitby, *Langmuir*, 2004, **20**, 1130–1137.
8 T. S. Horozov, R. Aveyard, J. H. Clint and B. P. Binks, *Langmuir*, 2003, **19**, 2822–2829.
9 J. Giermanska-Kahn, V. Schmitt, B. P. Binks and F. Leal-Calderon, *Langmuir*, 2002, **18**, 2515–2518.
10 Y. Lin, H. Skaff, T. Emrick, A. D. Dinsmore and T. P. Russell, *Science*, 2003, **299**, 226–229.
11 H. W. Duan, D. A. Wang, D. G. Kurth and H. Möhwald, *Angew. Chem., Int. Ed.*, 2004, **43**, 5639–5642.
12 H. Duan, D. Wang, N. S. Sobal, M. Giersig, D. G. Kurth and H. Möhwald, *Nano Lett.*, 2005, **5**, 949–952.
13 D. Y. Wang and H. Möhwald, *J. Mater. Chem.*, 2004, **14**, 459–468.
14 J. H. Schulmann and J. Leja, *Trans. Faraday Soc.*, 1954, **50**, 598–605.
15 R. Aveyard, J. H. Clint and T. S. Horozov, *Phys. Chem. Chem. Phys.*, 2003, **5**, 2398–2409.
16 G. Decher, *Science*, 1997, **277**, 1232–1237.
17 F. Caruso, R. A. Caruso and H. Möhwald, *Science*, 1998, **282**, 1111–1114.
18 J. N. Cha, H. Birkedal, L. E. Euliss, M. H. Bartl, M. S. Wong, T. J. Deming and G. D. Stucky, *J. Am. Chem. Soc.*, 2003, **125**, 8285–8289.
19 S. M. Marinakos, J. P. Novak, L. C. B. Ill, A. B. House, E. M. Edeki, J. C. Feldhaus and D. L. Feldheim, *J. Am. Chem. Soc.*, 1999, **121**, 8518–8522.
20 F. Tiarks, K. Landfester and M. Antonietti, *Langmuir*, 2001, **17**, 908–918.
21 F. Caruso, D. Trau, H. Möhwald and R. Renneberg, *Langmuir*, 2000, **16**, 1485–1488.
22 F. Caruso, W. J. Yang, D. Trau and R. Renneberg, *Langmuir*, 2000, **16**, 8932–8936.
23 C. Y. Gao, E. Donath, H. Möhwald and J. C. Shen, *Angew. Chem., Int. Ed.*, 2002, **41**, 3789–3793.
24 S. Schacht, Q. Hio, I. G. Voigt-Martin, G. D. Stucky and F. Schüth, *Science*, 1996, **273**, 768–771.
25 Q. Huo, P. Feng, F. Schüth and G. D. Stucky, *Chem. Mater.*, 1997, **9**, 14–17.
26 V. Tricoli, J. Sefcik and A. V. McCormic, *Langmuir*, 1997, **13**, 4193–4196.
27 Y. F. Lu, H. Y. Fan, A. Stump, T. L. Ward, T. Rieker and C. J. Brinker, *Nature*, 1999, **398**, 223–226.
28 C. E. Fowler, D. Khushalani and S. Mann, *Chem. Commun.*, 2001, 2028–2029.
29 A. D. Dinsmore, J. C. Crocker and A. G. Yodh, *Curr. Opin. Colloid Interface Sci.*, 1998, **3**, 5–11.
30 A. D. Dinsmore, M. F. Hsu, M. G. Nikolaides, M. Marquez, A. R. Bausch and D. A. Weitz, *Science*, 2002, **298**, 1006–1009.
31 H. Xu and W. A. Goedel, *Langmuir*, 2002, **18**, 2363–2367.
32 H. Xu and W. A. Goedel, *Angew. Chem., Int. Ed.*, 2003, **42**, 4694–4696.
33 H. Xu and W. A. Goedel, *Langmuir*, 2003, **19**, 4950–4952.
34 F. Mallwitz and W. A. Goedel, *Angew. Chem., Int. Ed.*, 2001, **40**, 2645–2647.
35 E. L. Chaikof, *Annu. Rev. Biomed. Eng.*, 1999, **1**, 103–127.
36 T. Joki, M. Machluf, A. Atala, J. Zhu, N. T. Seyfried, I. F. Dunn, T. Abe, R. S. Carroll and P. M. Black, *Nat. Biotechnol.*, 2001, **19**, 35–39.
37 R. P. Lanza, R. Langer and J. Vacanti, *Principles of Tissue Engineering*, Academic Press, San Diego, 2000.
38 T.-A. Read, D. R. Sorenson, R. Mahesparan, P. Enger, R. Timpl, B. R. Olsen, M. H. B. Hjelstuen, O. Haraldseth and R. Bjerkvig, *Nat. Biotechnol.*, 2001, **19**, 29–34.
39 T. A. Desai, D. J. Hansford and M. Ferrari, *Biomol. Eng.*, 2000, **17**, 23–36.
40 C. B. Murray, C. R. Kagan and M. G. Bawendi, *Annu. Rev. Mater. Sci.*, 2000, **30**, 545–610.
41 C. B. Murray, C. R. Kagan and M. G. Bawendi, *Science*, 1995, **270**, 1335–1338.
42 P. S. Shah, M. B. Sigman, Jr., C. A. Stowell, K. T. Lim, K. P. Johnston and B. A. Korgel, *Adv. Mater.*, 2003, **15**, 971–974.
43 B. A. Korgel, *Science*, 2004, **303**, 1308–1309.
44 C. B. Murray, D. J. Norris and M. G. Bawendi, *J. Am. Chem. Soc.*, 1993, **115**, 8706–8715.
45 Y. Lin, A. Böker, H. Skaff, D. Cookson, A. D. Dinsmore, T. Emrick and T. P. Russell, *Langmuir*, 2005, **21**, 191–194.
46 Y. Lin, H. Skaff, A. Böker, A. D. Dinsmore, T. Emrick and T. P. Russell, *J. Am. Chem. Soc.*, 2003, **125**, 12690–12691.
47 A. Kulak, S. A. Davis, E. Dujardin and S. Mann, *Chem. Mater.*, 2003, **15**, 528–535.
48 L. Dai, R. Sharma and C. Y. Wu, *Langmuir*, 2005, **21**, 2641–2643.
49 H. Skaff, Y. Lin, R. Tangirala, K. Breitenkamp, A. Böker, T. P. Russell and T. Emrick, *Adv. Mater.*, 2005, **17**, 2082–2086.
50 Z. Y. Tang, Z. L. Zhang, Y. Wang, S. C. Glotzer and N. A. Kotov, *Science*, 2006, **314**, 274–278.
51 C. Y. Jiang, S. Markutsya, Y. Pikus and V. V. Tsukruk, *Nat. Mater.*, 2004, **3**, 721–728.
52 B. P. Binks and P. D. I. Fletcher, *Langmuir*, 2001, **17**, 4708–4710.
53 A. Perro, S. Reculusa, S. Ravaine, E. B. Bourgeat-Lami and E. Duguet, *J. Mater. Chem.*, 2005, **15**, 3745–3760.
54 R. Erhardt, A. Böker, H. Zettl, H. Kaya, W. Pyckhout-Hintzen, G. Krausch, V. Abetz and A. H. E. Müller, *Macromolecules*, 2001, **34**, 1069–1075.
55 R. Erhardt, M. F. Zhang, A. Böker, H. Zettl, C. Abetz, P. Frederik, G. Krausch, V. Abetz and A. H. E. Müller, *J. Am. Chem. Soc.*, 2003, **125**, 3260–3267.
56 S. Förster and M. Antonietti, *Adv. Mater.*, 1998, **10**, 195–217.
57 S. Schrage, R. Sigel and H. Schlaad, *Macromolecules*, 2003, **36**, 1417–1420.
58 T. Teranishi, Y. Inoue, M. Nakaya, Y. Oumi and T. Sano, *J. Am. Chem. Soc.*, 2004, **126**, 9914–9915.
59 H. W. Gu, R. K. Zheng, X. X. Zhang and B. Xu, *J. Am. Chem. Soc.*, 2004, **126**, 5664–5665.
60 Y. Li, Q. Zhang, A. V. Nurmikko and S. H. Sun, *Nano Lett.*, 2005, **5**, 1689–1692.
61 E. Duguet, C. Poncet-Legrand, S. Raviane, E. Bourgeat-Lami, S. Reculusa, C. Mingotaud, M. H. Delville and F. Pereira, WO 2005/049195, France, 2005.
62 L. Hong, S. Jiang and S. Granick, *Langmuir*, 2006, **22**, 9495–9499.
63 Z. F. Li, D. Y. Lee, M. F. Rubner and R. E. Cohen, *Macromolecules*, 2005, **38**, 7876–7879.
64 N. Glaser, D. Adams, A. Böker and G. Krausch, *Langmuir*, 2006, **22**, 5227–5229.
65 H. Yu, M. Chen, P. M. Rice, S. X. Wang, R. L. White and S. H. Sun, *Nano Lett.*, 2005, **5**, 379–382.
66 X. G. Peng, L. Manna, W. D. Yang, J. Wickham, E. Scher, A. Kadavanich and A. P. Alivisatos, *Nature*, 2000, **404**, 59–61.
67 Z. A. Peng and X. G. Peng, *J. Am. Chem. Soc.*, 2002, **124**, 3343–3353.
68 V. F. Puntes, K. M. Krishnan and A. P. Alivisatos, *Science*, 2001, **291**, 2115–2117.
69 D. V. Talapin, E. V. Shevchenko, C. B. Murray, A. Kornowski, S. Forster and H. Weller, *J. Am. Chem. Soc.*, 2004, **126**, 12984–12988.
70 H. Maeda and Y. Maeda, *Phys. Rev. Lett.*, 2003, **90**, 018303.
71 N. R. Jana, *Angew. Chem., Int. Ed.*, 2004, **43**, 1536–1540.
72 S. Paul, C. Pearson, A. Molloy, M. A. Cousins, M. Green, S. Kolliopoulou, P. Dimitrakis, P. Normand, D. Tsoukalas and M. C. Petty, *Nano Lett.*, 2003, **3**, 533–536.
73 M. G. Basavaraj, G. G. Fuller, J. Fransaer and J. Vermant, *Langmuir*, 2006, **22**, 6605–6612.
74 B. P. Khanal and E. R. Zubarev, *Angew. Chem., Int. Ed.*, 2007, **46**, 2195–2198.
75 L. C. Dong and D. T. Johnson, *Langmuir*, 2005, **21**, 3838–3849.
76 E. P. Lewandowski, P. C. Searson and K. J. Stebe, *J. Phys. Chem. B*, 2006, **110**, 4283–4290.
77 J. He, Q. Zhang, S. Gupta, P. Thiyagarajan, T. Emrick and T. P. Russell, *Small*, 2007, **3**, 1214–1217.
78 B. P. Binks, *Curr. Opin. Colloid Interface Sci.*, 2001, **6**, 17–21.
79 W. H. Binder, *Angew. Chem., Int. Ed.*, 2005, **44**, 5172–5175.

80 W. U. Huynh, J. J. Dittmer and A. P. Alivisatos, *Science*, 2002, **295**, 2425–2427.
81 X. F. Duan, Y. Huang, Y. Cui, J. F. Wang and C. M. Lieber, *Nature*, 2001, **409**, 66–69.
82 Y. Huang, X. F. Duan, Q. Q. Wei and C. M. Lieber, *Science*, 2001, **291**, 630–633.
83 G. M. Whitesides and B. Grzybowski, *Science*, 2002, **295**, 2418–2421.
84 A. Böker, Y. Lin, K. Chiapperini, R. Horowitz, M. Thompson, V. Carreon, T. Xu, C. Abetz, H. Skaff, A. D. Dinsmore, T. Emrick and T. P. Russell, *Nat. Mater.*, 2004, **3**, 302–306.
85 Y. Boontongkong and R. E. Cohen, *Macromolecules*, 2002, **35**, 3647–3652.
86 B. H. Sohn and B. H. Seo, *Chem. Mater.*, 2001, **13**, 1752–1757.
87 B.-H. Sohn, J.-M. Choi, S. I. Yoo, S.-H. Yun, W.-C. Zin, J. C. Jung, M. Kanehara, T. Hirata and T. Teranishi, *J. Am. Chem. Soc.*, 2003, **125**, 6368–6369.
88 J. Spatz, S. Mössmer, M. Möller, M. Kocher, D. Neher and G. Wegner, *Adv. Mater.*, 1998, **10**, 473–475.
89 W. A. Lopes and H. M. Jaeger, *Nature*, 2001, **414**, 735–738.
90 R. B. Cheyne and M. G. Moffit, *Macromolecules*, 2007, **40**, 2046–2057.
91 R. B. Thompson, V. V. Ginzburg, M. W. Matsen and A. C. Balazs, *Science*, 2001, **292**, 2469–2472.
92 J. Y. Lee, Z. Shou and A. C. Balazs, *Phys. Rev. Lett.*, 2003, **91**, 136103.
93 J. Y. Lee, Z. Shou and A. C. Balazs, *Macromolecules*, 2003, **36**, 7730–7739.
94 M. R. Bockstaller, Y. Lapetnikov, S. Margel and E. L. Thomas, *J. Am. Chem. Soc.*, 2003, **125**, 5276–5277.
95 J. J. Chiu, B. J. Kim, E. J. Kramer and D. J. Pine, *J. Am. Chem. Soc.*, 2005, **127**, 5036–5037.
96 B. J. Kim, J. J. Chiu, G. R. Yi, D. J. Pine and E. J. Kramer, *Adv. Mater.*, 2005, **17**, 2618–2622.
97 H. Chung, K. Ohno, T. Fukuda and R. J. Composto, *Nano Lett.*, 2005, **5**, 1878–1882.
98 B. J. Kim, J. Bang, C. J. Hawker and E. J. Kramer, *Macromolecules*, 2006, **39**, 4108–4114.
99 B. J. Kim, S. Given-Beck, J. Bang, C. J. Hawker and E. J. Kramer, *Macromolecules*, 2007, **40**, 1796–1798.
100 Y. Lin, A. Böker, J. He, K. Sill, H. Xiang, C. Abetz, X. Li, J. Wang, T. Emrick, S. Long, Q. Wang, A. Balazs and P. Russell Thomas, *Nature*, 2005, **434**, 55–59.
101 J. He, R. Tangirala, T. Emrick, T. P. Russell, A. Böker, X. Li and J. Wang, *Adv. Mater.*, 2007, **19**, 381–385.
102 S. Tyagi, J. Y. Lee, G. A. Buxton and A. C. Balazs, *Macromolecules*, 2004, **37**, 9160–9168.
103 J. Y. Lee, G. A. Buxton and A. C. Balazs, *J. Chem. Phys.*, 2004, **121**, 5531–5540.
104 S. Gupta, Q. L. Zhang, T. Emrick, A. C. Balazs and T. P. Russell, *Nat. Mater.*, 2006, **5**, 229–233.
105 A. C. Balazs, T. Emrick and T. P. Russell, *Science*, 2006, **314**, 1107–1110.
106 J. Y. Lee, Q. L. Zhang, T. Emrick and A. J. Crosby, *Macromolecules*, 2006, **39**, 7392–7396.
107 J. C. Smith, K. B. Lee, Q. Wang, M. G. Finn, J. E. Johnson, M. Mrksich and C. A. Mirkin, *Nano Lett.*, 2003, **3**, 883–886.
108 C. B. Mao, C. E. Flynn, A. Hayhurst, R. Sweeney, J. F. Qi, G. Georgiou, B. Iverson and A. M. Belcher, *Proc. Natl. Acad. Sci. U. S. A.*, 2003, **100**, 6946–6951.
109 C. L. Cheung, J. A. Camarero, B. W. Woods, T. W. Lin, J. E. Johnson and J. J. De Yoreo, *J. Am. Chem. Soc.*, 2003, **125**, 6848–6849.
110 K. S. Raja, Q. Wang, M. J. Gonzalez, M. Manchester, J. E. Johnson and M. G. Finn, *Biomacromolecules*, 2003, **4**, 472–476.
111 S. W. Lee, S. K. Lee and A. M. Belcher, *Adv. Mater.*, 2003, **15**, 689–692.
112 E. Dujardin, C. Peet, G. Stubbs, J. N. Culver and S. Mann, *Nano Lett.*, 2003, **3**, 413–417.
113 M. Allen, D. Willits, J. Mosolf, M. Young and T. Douglas, *Adv. Mater.*, 2002, **14**, 1562–1565.
114 E. Gillitzer, D. Willits, M. Young and T. Douglas, *Chem. Commun.*, 2002, 2390–2391.
115 S. W. Lee, C. B. Mao, C. E. Flynn and A. M. Belcher, *Science*, 2002, **296**, 892–895.
116 T. Douglas, E. Strable, D. Willits, A. Aitouchen, M. Libera and M. Young, *Adv. Mater.*, 2002, **14**, 415–418.
117 Q. Wang, T. W. Lin, L. Tang, J. E. Johnson and M. G. Finn, *Angew. Chem., Int. Ed.*, 2002, **41**, 459–462.
118 C. E. Fowler, W. Shenton, G. Stubbs and S. Mann, *Adv. Mater.*, 2001, **13**, 1266–1269.
119 S. R. Hall, W. Shenton, H. Engelhardt and S. Mann, *ChemPhysChem*, 2001, **2**, 184–186.
120 S. R. Whaley, D. S. English, E. L. Hu, P. F. Barbara and A. M. Belcher, *Nature*, 2000, **405**, 665–668.
121 S. Mann, W. Shenton, M. Li, S. Connolly and D. Fitzmaurice, *Adv. Mater.*, 2000, **12**, 147–150.
122 T. Douglas and M. Young, *Adv. Mater.*, 1999, **11**, 679–681.
123 W. Shenton, T. Douglas, M. Young, G. Stubbs and S. Mann, *Adv. Mater.*, 1999, **11**, 253–256.
124 T. Douglas and M. Young, *Nature*, 1998, **393**, 152–155.
125 S. Mann, D. D. Archibald, J. M. Didymus, T. Douglas, B. R. Heywood, F. C. Meldrum and N. J. Reeves, *Science*, 1993, **261**, 1286–1292.
126 V. A. Fonoberov and A. A. Balandin, *Nano Lett.*, 2005, **5**, 1920–1923.
127 W. L. Liu, K. Alim, A. A. Balandin, D. M. Mathews and J. A. Dodds, *Appl. Phys. Lett.*, 2005, **86**, 253108.
128 K. T. Nam, B. R. Peelle, S. W. Lee and A. M. Belcher, *Nano Lett.*, 2004, **4**, 23–27.
129 P. J. Yoo, K. T. Nam, J. F. Qi, S. K. Lee, J. Park, A. M. Belcher and P. T. Hammond, *Nat. Mater.*, 2006, **5**, 234–240.
130 P. Fromherz, *Nature*, 1971, **231**, 267–268.
131 B. K. Jap, M. Zulauf, T. Scheybani, A. Hefti, W. Baumeister, U. Aebi and A. Engel, *Ultramicroscopy*, 1992, **46**, 45–84.
132 K. Aoyama, K. Ogawa, Y. Kimura and Y. Fujiyoshi, *Ultramicroscopy*, 1995, **57**, 345–354.
133 E. E. Uzgiris and R. D. Kornberg, *Nature*, 1983, **301**, 125–129.
134 T. Scheybani, H. Yoshimura, W. Baumeister and K. Nagayama, *Langmuir*, 1996, **12**, 431–435.
135 I. Yamashita, *Thin Solid Films*, 2001, **393**, 12–18.
136 H. Yoshimura, T. Scheybani, W. Baumeister and K. Nagayama, *Langmuir*, 1994, **10**, 3290–3295.
137 A. S. Dimitrov, M. Yamaki and K. Nagayama, *Langmuir*, 1995, **11**, 2682–2688.
138 M. Yamaki, K. Matsubara and K. Nagayama, *Langmuir*, 1993, **9**, 3154–3158.
139 H. Yoshimura, M. Matsumoto, S. Endo and K. Nagayama, *Ultramicroscopy*, 1990, **32**, 265–274.
140 E. Adachi and K. Nagayama, *Langmuir*, 1996, **12**, 1836–1839.
141 G. P. Lomonossoff, M. Shanks, C. L. Holness, A. J. Maule, D. Evans, Z. Chen, C. V. Stauffacher and J. E. Johnson, *Proc. Phytochem. Soc. Eur.*, 1991, **32**, 76–91.
142 G. P. Lomonossoff and J. E. Johnson, *Prog. Biophys. Mol. Biol.*, 1991, **55**, 107–137.
143 D. J. Siler, J. Babcock and G. Bruening, *Virology*, 1976, **71**, 560–567.
144 T. Lin, Z. Chen, R. Usha, C. V. Stauffacher, J.-B. Dai, T. Schmidt and J. E. Johnson, *Virology*, 1999, **265**, 20–34.
145 P. Aisen and I. Listowsky, *Annu. Rev. Biochem.*, 1980, **49**, 357–393.
146 T. Hikono, Y. Uraoky, T. Fuyuki and I. Yamashita, *Jpn. J. Appl. Phys., Part 2*, 2003, **42**, 398–399.
147 Q. Wang, T. Lin, L. Tang, J. E. Johnson and M. G. Finn, *Angew. Chem., Int. Ed.*, 2002, **41**, 459–462.
148 Q. Wang, E. Kaltgrad, T. Lin, J. E. Johnson and M. G. Finn, *Chem. Biol.*, 2002, **9**, 805–811.
149 K. A. Beningo, C. M. Lo and Y. L. Wang, in *Methods in Cell-Matrix Adhesion*, 2002, Academic Press, San Diego, pp. 325–339.
150 A. Chatterji, W. F. Ochoa, M. Paine, B. R. Ratna, J. E. Johnson and T. W. Lin, *Chem. Biol.*, 2004, **11**, 855–863.
151 C. Porta, V. E. Spall, T. Lin, J. E. Johnson and G. P. Lomonossoff, *Intervirology*, 1996, **39**, 79–84.
152 K. M. Taylor, T. Lin, C. Porta, A. G. Mosser, H. A. Giesing, G. P. Lomonossoff and J. E. Johnson, *J. Mol. Recognit.*, 2000, **13**, 71–82.
153 G. P. Lomonossoff and W. D. O. Hamilton, *Curr. Top. Microbiol. Immunol.*, 1999, **240**, 177–189.

154 A. S. Blum, C. M. Soto, C. D. Wilson, J. D. Cole, M. Kim, B. Gnade, A. Chatterji, W. F. Ochoa, T. W. Lin, J. E. Johnson and B. R. Ratna, *Nano Lett.*, 2004, **4**, 867–870.
155 D. N. Chasteen and P. M. Harrison, *J. Struct. Biol.*, 1999, **126**, 182–194.
156 T. D. Martin, S. A. Monheit, R. J. Niichel, S. C. Peterson, C. H. Campbell and D. C. Zapien, *J. Electroanal. Chem.*, 1997, **420**, 279–290.
157 K. K. W. Wong and S. Mann, *Adv. Mater.*, 1996, **8**, 928–932.
158 K. K. W. Wong, T. Douglas, S. Gider, D. D. Awschalom and S. Mann, *Chem. Mater.*, 1998, **10**, 279–285.
159 I. Yamashita, *Thin Solid Films*, 2001, **393**, 12–18.
160 D. C. Zapien and M. A. Johnson, *J. Electroanal. Chem.*, 2000, **494**, 114–120.
161 J. T. Russell, Y. Lin, A. Böker, L. Su, P. Carl, H. Zettl, J. B. He, K. Sill, R. Tangirala, T. Emrick, K. Littrell, P. Thiyagarajan, D. Cookson, A. Fery, Q. Wang and T. P. Russell, *Angew. Chem., Int. Ed.*, 2005, **44**, 2420–2426.
162 K. K. W. Wong, N. T. Whilton, T. Douglas, S. Mann and H. Cölfen, *Chem. Commun.*, 1998, 1621–1622.
163 K. K. W. Wong, H. Colfen, N. T. Whilton, T. Douglas and S. Mann, *J. Inorg. Biochem.*, 1999, **76**, 187–195.
164 Q. Wang, T. Chan, R. Hilgraf, V. V. Fokin, K. B. Sharpless and M. G. Finn, *J. Am. Chem. Soc.*, 2003, **125**, 3192–3193.
165 K. Wetz and R. R. Crichton, *Eur. J. Biochem.*, 1976, **61**, 545–550.